J. Fluid Mech. (2007), *vol.* 593, *pp.* 93–129. © 2007 Cambridge University Press
doi:10.1017/S0022112007008385 Printed in the United Kingdom

Transverse-jet shear-layer instabilities. Part 1. Experimental studies

S. MEGERIAN, J. DAVITIAN, L. S. de B. ALVES, AND A. R. KARAGOZIAN†

Department of Mechanical and Aerospace Engineering,
University of California, Los Angeles, Los Angeles, CA 90095-1597, USA

(Received 12 September 2006 and in revised form 18 July 2007)

This study provides a detailed exploration of the near-field shear-layer instabilities associated with a gaseous jet injected normally into crossflow, also known as the transverse jet. Jet injection from nozzles which are flush as well as elevated with respect to the tunnel wall are explored experimentally in this study, for jet-to-crossflow velocity ratios R in the range $1 \lesssim R \leqslant 10$ and with jet Reynolds numbers of 2000 and 3000. The results indicate that the nature of the transverse jet instability is significantly different from that of the free jet, and that the instability changes in character as the crossflow velocity is increased. Dominant instability modes are observed to be strengthened, to move closer to the jet orifice, and to increase in frequency as crossflow velocity increases for the regime $3.5 < R \leqslant 10$. The instabilities also exhibit mode shifting downstream along the jet shear layer for either nozzle configuration at these moderately high values of R. When R is reduced below 3.5 in the flush injection experiments, single-mode instabilities are dramatically strengthened, forming almost immediately within the shear layer in addition to harmonic and subharmonic modes, without any evidence of mode shifting. Under these conditions, the dominant and initial mode frequencies tend to decrease with increasing crossflow. In contrast, the instabilities in the elevated jet experiments are weakened as R is reduced below about 4, probably owing to an increase in the vertical coflow magnitude exterior to the elevated nozzle, until R falls below 1.25, at which point the elevated jet instabilities become remarkably similar to those for the flush injected jet. Low-level jet forcing has no appreciable influence on the shear-layer response when these strong modes are present, in contrast to the significant influence of low-level forcing otherwise. These studies suggest profound differences in transverse-jet shear-layer instabilities, depending on the flow regime, and help to explain differences previously observed in transverse jets controlled by strong forcing.

1. Introduction and background

The flow field associated with the round jet injected normally into crossflow is one that has been extensively studied (Kamotani & Greber 1972; Fric & Roshko 1994; Kelso, Lim & Perry 1996; Smith & Mungal 1998) because of its widespread applications, particularly in propulsion systems (Holdeman 1993), and its superior mixing characteristics when compared with the free jet issuing into quiescent surroundings (Broadwell & Breidenthal 1984; Karagozian 1986; Margason 1993).

† Author to whom correspondence should be addressed: ark@seas.ucla.edu.

https://doi.org/10.1017/S0022112007008385 Published online by Cambridge University Press

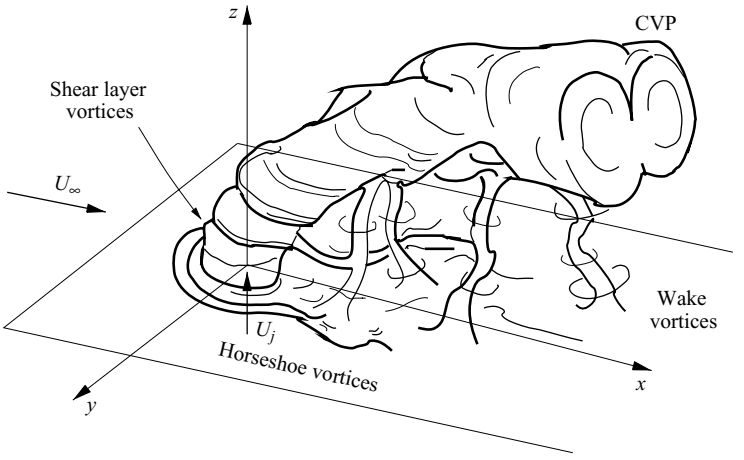


FIGURE 1. Schematic of the transverse jet, introduced flush with respect to the injection wall, and relevant vortical structures. From Fric & Roshko (1994).

Transverse jets find applications as dilution air jets for gas turbine engines, where such jets can lead to improved control of temperature pattern factor and NO_x emissions, in fuel and/or overfire air jets in utility burners and hazardous waste incinerators, and in thrust vectoring jets in high-speed aerospace systems. The ability to control the penetration, spreading and mixing associated with this flow field is highly beneficial for the design and optimization of the performance of such devices.

1.1. *Vortex systems in transverse jets*

Figure 1 shows the dominant vortical structures associated with the jet in crossflow (JICF). The JICF typically consists of a jet of mean velocity U_j issuing perpendicularly into a crossflow of velocity U_∞, with the jet exiting either flush from an orifice embedded within a wall (figure 1), or from an elevated pipe or nozzle. The transverse jet is a more complicated flow field than the free jet in quiescent surroundings owing to its interaction with the crossflow and, for the case of the flush jet in crossflow, interaction of the jet with the wall boundary layer. Among the parameters used to characterize this flow field are the jet-to-crossflow momentum flux ratio, J, the jet-to-crossflow velocity ratio R, and the jet Reynolds number Re, which is based on the jet's inner diameter D. Either R or J is typically used to scale the trajectory of the JICF (Smith & Mungal 1998), but there is a relatively weak dependence of trajectory on jet Reynolds number as well (Yuan & Street 1998). In the limit of isodensity jets in crossflow, $J = R^2$.

The fundamental dynamics of the JICF are dominated by a complex inter-related set of vortex systems, some of which are shown conceptually in figure 1. These include the counter-rotating vortex pair (CVP), observed to dominate the jet cross-section, especially in the far field (Kamotani & Greber 1972) but with evidence of its near field generation through the distortion of the vorticity in the jet shear layer (Kelso *et al.* 1996; Smith & Mungal 1998; Cortelezzi & Karagozian 2001). Mixing enhancement by the JICF is often associated with development, sustenance, and eventual breakdown of the CVP structures (Broadwell & Breidenthal 1984; Karagozian 1986; Margason 1993). For the transverse jet injected flush from a wall, there are additionally horseshoe vortices (Kelso & Smits 1995), which form in the plane of the injection wall and surround the upstream portion of the jet, and upright

https://doi.org/10.1017/S0022112007008385 Published online by Cambridge University Press

wake vortices (Fric & Roshko 1994), which are thought to be initiated within the wall boundary layer and evolve periodically about and beyond the JICF. Fric & Roshko (1994) indicate that these wake vortices allow fluid to be drawn from the boundary layer into the jet itself, with a 'bursting of the boundary layer fluid into the wake structures' being most pronounced at $R = 4$. The horseshoe vortex system is observed to have oscillatory as well as stationary modes that correlate with R and the jet Reynolds number (Kelso & Smits 1995); in some cases, the oscillatory modes have the same Strouhal number as that for the wake vortices.

Because the counter-rotating vortex pair is thought to be associated with enhanced overall mixing efficiency for the transverse jet, the formation and evolution of the CVP have been the focus of a number of studies over the past several decades, including experimental exploration (Kamotani & Greber 1972; Moussa, Trischka & Eskinazi 1977; Andreopoulos 1985; Kelso *et al.* 1996; Smith & Mungal 1998) as well as numerical simulation (Yuan & Street 1998; Cortelezzi & Karagozian 2001). Experimental studies in the near field have suggested that the CVP is formed by the shear layer emanating from the jet nozzle or pipe. The experiments of Kelso *et al.* (1996) in both water and air suggest that periodic vortex ring roll-up from the nozzle occurs for the jet in crossflow, similar to that which occurs in the free jet, yet superposed on this process is a re-orientation of this shear-layer vorticity imposed by the crossflow which leads to a folding of the cylindrical vortex sheet and the initiation of the dominant CVP structure. Experiments on flush-injected transverse jets by Peterson & Plesniak (2004) suggest that vortical structures generated within the jet orifice arising from asymmetry in the jet's supply flow can, in fact, constructively or destructively interact ultimately with the CVP, thus affecting its coherence. Hence the nature of flow interactions in the near-field of the transverse-jet shear layer and possibly its associated instabilities can have a significant influence on the CVP, and thus can affect the jet's mixing properties.

1.2. *Transverse-jet shear-layer instabilities*

The transverse jet's shear-layer vortices are generally thought to result from a Kelvin–Helmholtz instability near the jet exit (Fric & Roshko 1994; Kelso & Smits 1995; Kelso *et al.* 1996; Yuan & Street 1998). Depending on the nature of the flow exiting the jet nozzle or pipe, the spatial profile of the jet's exit velocity can have an inflection point, suggesting the potential for the development of this instability. Vorticity in the shear layer rolls up at this upstream edge of the jet, forming vortices which gain strength and can roll up periodically along the upstream side of the jet, with evidence of pairing and merger (Fric & Roshko 1994). Andreopoulos (1985) reports that these shear-layer toroidal vortices have the same sign of vorticity and the same length scale as the boundary layer inside the jet pipe.

In contrast, Blanchard, Brunet & Merlen (1999) argue that the near-field instabilities for the JICF are not of the Kelvin–Helmholtz type, owing to the shear between the jet and cross-stream, but rather are of an elliptical nature, strongly influenced by the near-field formation and longitudinal evolution of the CVP and its effect on transverse eddy structures. Yet the experiments by Blanchard *et al.* are for a thin slit in crossflow, rather than the round jet, as is more commonly studied, and their experiments are performed at very low jet Reynolds numbers (below 130 based on the jet's hydraulic diameter). The liquid experiments of Camussi, Guj & Stella (2002), using particle image velocimetry, are conducted at $150 \lesssim Re \lesssim 450$ and at relatively low jet-to-crossflow velocity ratios ($1.5 \leqslant R \leqslant 4.5$). These workers also suggest the onset of the shear-layer instability in this regime is driven by mechanisms which are 'different

https://doi.org/10.1017/S0022112007008385 Published online by Cambridge University Press

Study	Jet exit profile	*Re*	*R*	*St*
Fric & Roshko (1994)	Top hat	7700	2	1.7 (approx.)
Rudman (1996)	Top hat	2000	5	0.7–0.75
Kelso *et al.* (1996)	Fully developed	13 600	2.2	0.30
Smith & Mungal (1998)	Top hat	16 600	5	2.0 (approx.)
Camussi *et al.* (2002)	Fully developed	220	2.2	0.3
Narayanan *et al.* (2003)	Developed	5000	6	0.1 (broad peak)

TABLE 1. Approximate values of Strouhal numbers associated with the transverse jet near-field shear layer as documented in the literature.

from the Kelvin–Helmholtz instability of the [free] jet shear layer', since the 'whole jet flow oscillates' before vortex roll-up apears. They suggest that the formation of ring-like vortices in the transverse-jet shear layer arises not from a Kelvin–Helmholtz instability process, but rather from a 'waving of the jet flow'.

At low jet-to-crossflow velocity ratios ($R \leqslant 2.3$) and jet Reynolds numbers ($Re \approx 2100$) for a round fully developed liquid jet injected flush from a straight pipe, Kelso *et al.* (1996) observe that the laminar jet shear layer exhibits a Kelvin–Helmholtz-like instability at about 3 jet diameters above the exit. The presence of a 'hovering vortex' is also suggested, one that wraps around the front and sides of the jet but which the authors distinguish from the horseshoe vortices, which lie much closer to the injection wall, upstream of the jet. Kelso *et al.* write that, as the crossflow velocity is increased, 'the Kelvin–Helmholtz-like instability [associated with the jet shear layer] occurs progressively closer to the jet exit' until an interaction with the hovering vortex, which itself becomes unsteady and begins to shed vortices downstream of the jet. Under these very low R conditions, they see that 'the shear layer roll-up is of large scale, is periodic, and occurs near or within the pipe exit'. This transition in the nature of the shear layer may be similar to what Camussi *et al.* (2002) call a 'waving of the jet flow'.

Jet shear-layer instabilities in general can be quantified in terms of a Strouhal number, $St = fD/U_j$, where f is the frequency of the instability of interest. Yet there are few studies, either experimental or theoretical/numerical, that have systematically quantified dominant Strouhal numbers associated with transverse-jet shear-layer vortices for a range of conditions. Table 1 presents approximate values of Strouhal numbers associated with the transverse jet's upstream shear layer that are available (or quantifiable from data) in the literature. The studies by Rudman (1996), Camussi *et al.* (2002), and Narayanan, Barooah & Cohen (2003) provide spectral data; others provide estimated values or images from which vortex roll-up frequencies may be roughly estimated. The rather wide range of Strouhal numbers for the range of conditions explored is in part what has led to our present experimental exploration of this instability.

For the free jet in quiescent surroundings, experiments over many years (e.g. Kibens 1981; Ho & Huerre 1984) indicate that the jet's 'preferred modes,' which correspond to the most energetic disturbance near the end of the jet's potential core, range in Strouhal number from about 0.24 to 0.51. Yet Petersen & Samet (1988) note that these values of St for the free jet can be dependent on the experimental configuration, and also that the strong dependence of the Strouhal number on the local jet shear-layer momentum thickness suggests an evolutionary nature of the instability. They demonstrate the development of the instability from spectra which show shear-layer

https://doi.org/10.1017/S0022112007008385 Published online by Cambridge University Press

peaks close to the jet exit, then as one moves downstream, subharmonic resonances and pairings, eventually leading to the dominance of a 'preferred mode' near the end of the potential core. The character of the spatial evolution of the free-jet instability is consistent with its classification as a convective instability (Huerre & Monkewitz 1990).

1.3. *The forced jet in crossflow*

An understanding of transverse jet shear-layer instabilities can have a profound impact on jet control. Active control of the penetration and mixing processes associated with the transverse jet may be accomplished through temporal excitation of the jet flow issuing from the orifice. Experiments on pulsed transverse jets by other groups (Vermeulen, Grabinski & Ramesh 1992; Johari, Pacheco-Tougas & Hermanson 1999; Eroglu & Breidenthal 2001; Narayanan *et al.* 2003) demonstrate that temporally varying the jet velocity allows jet penetration, spread, and/or mixing to be enhanced at specific conditions of excitation. For example, in the study of fully modulated liquid jets in crossflow with square-wave excitation by Johari *et al.* (1999), the maximum jet penetration occurs at a forcing frequency corresponding to a jet Strouhal number of 0.004 for $R = 5$. Such maxima generally occur for low-duty cycles, of the order $\alpha = 20\,\%$, where the duty cycle α is defined as the temporal pulse width τ during a given cycle divided by the period T. On the other hand, recent gaseous experiments on the forced JICF with $R = 6$ and $Re = 5000$ by Narayanan *et al.* (2003) indicate significant jet response at low-amplitude sinusoidal forcing, with an amplitude less than 30 % of the mean jet velocity. In these studies, the greatest enhancement in mixing (by about 30–40 %) occurs during forcing at a jet Strouhal number of 0.2, which is twice that of their unforced transverse jet's preferred mode. Yet for these conditions, there is only a marginal increase in transverse-jet penetration. In further contrast, low-amplitude sinusoidal forcing of the gaseous jet in crossflow by Kelso *et al.* (1996), at an amplitude that is 10 % of the jet's mean velocity, suggests that the global structure of the interaction between jet and crossflow is not changed unless the jet is forced very near the Strouhal number associated with the shear layer of the unforced JICF (for a gaseous jet with $R = 2.2$ and $Re = 13,640$). Relatively little alteration in transverse-jet penetration or spread is attained through such forcing, however.

Systematic experimental work involving controlled transverse jets at UCLA (Schuller *et al.* 1999; King 2002; M'Closkey *et al.* 2002; Shapiro 2003; Shapiro *et al.* 2006) has focused on the acoustically forced, round gaseous jet injected perpendicularly into a low-speed wind tunnel. A feedforward controller or dynamical compensator is developed in the forced-jet experiments to produce a more accurately prescribed temporal waveform at the jet exit. Details on and demonstration of the controller are provided in M'Closkey *et al.* (2002), whereas the experimental apparatus in these tests, similar to that in the present study, is described in detail in § 2.

At the relatively low jet-to-crossflow velocity ratios explored in these early studies ($2.56 \leqslant R \leqslant 4.0$), forced sinusoidal excitation of the jet is seen to have relatively little influence on jet response, even with very large-amplitude excitation, exceeding 75 % of the mean jet velocity. This is seen irrespective of the single frequency of excitation i.e. whether forced at Strouhal numbers that coincide with those of the unforced jet shear layer, are at subharmonics thereof, or are at other frequencies. On the other hand, in many cases, square-wave excitation at subharmonics of the unforced shear-layer mode (and with the same root mean square of the velocity excitation as in sinusoidal forcing) yields significant increases in the jet penetration and spread

https://doi.org/10.1017/S0022112007008385 Published online by Cambridge University Press

(M'Closkey *et al.* 2002). Distinct, deeply penetrating vortical structures are formed periodically, creating much greater overall jet penetration and, for relatively low-duty cycles, a bifurcated jet structure. Systematic studies of the specific conditions (forcing frequencies, duty cycles for square-wave excitation, amplitudes of excitation) which lead to enhancement of jet penetration and spread indicate that specific values of the temporal pulsewidth τ can provide optimal merger and penetration of vortical structures (Shapiro *et al.* 2006). An interpretation of the time scales associated with this optimization uses the ideas of Gharib, Rambod & Shariff (1998) on the existence of a universal time scale required for coherent vortex ring formation.

The observations in Shapiro *et al.* (2006) suggest that subharmonic square-wave forcing of the transverse jet may enhance the merger and pairing of vortical structures in such a way as to augment the generation of deeply penetrating large-scale structures. On the other hand, there is no significant increase in transverse-jet response (M'Closkey *et al.* 2002) when the jet is excited sinusoidally at the subharmonics of the dominant shear-layer mode for low values of R (below 4), even at large amplitudes of forcing. Yet as noted previously, some workers have seen that at higher values of R for the gaseous transverse jet (e.g. $R = 6$ by Narayanan *et al.* 2003), even low-level sinusoidal excitation at or above the frequency of the shear-layer mode can lead to improved transverse jet mixing and spread.

Thus it is of interest to quantify and understand, for a range of jet and crossflow conditions, the nature of transverse-jet shear-layer instability modes and to use this knowledge to interpret prior observations in forced-jet experiments. This shear-layer-stability exploration is being pursued both experimentally and theoretically. A description of and results for the experiments appear in the present paper, while a linear stability analysis of the transverse-jet shear layer for relatively large jet-to-crossflow velocity ratios ($R > 4$) is described in Part 2 (Alves, Kelly & Karagozian 2007*b*). A prior paper (Alves *et al.* 2007*a*) describes a linear stability analysis for the transverse jet using an irrotational base flow, which reveals relevant information on the theoretical underpinnings of the instabilities as well as the initiation of asymmetries in the transverse jet, even for very large jet-to-crossflow velocity ratios ($R > 10$).

2. Experimental set-up

Figure 2 shows the present experimental set-up. A nitrogen jet issued perpendicularly into the crossflow of air at room temperature, with an electric motor driving a compressor which introduced ambient air into the wind tunnel. The compressor was isolated from the wind tunnel so as to minimize the influence of its mechanical vibrations on the experiment. The crossflow air passed through a series of screens and honeycomb flow straighteners before entering a contraction (with area ratio 9:1) upstream of the test section. The test section was $12\,\text{cm} \times 12\,\text{cm}$ in cross-section, with a tunnel length four times that shown in figure 2 (approximately 1 m in total). Crossflow speeds upstream of the jet ranged from 1.3 to $7.2\,\text{m}\,\text{s}^{-1}$, with turbulence intensities less than 1.5 %. Quartz windows were fitted in two perpendicular sidewalls of the wind-tunnel test section for optical access. The jet nozzle was situated at the bottom of the tunnel, with its exit plane located 9.5 cm downstream of the end of the tunnel contraction.

Two alternative round-jet nozzles were explored, one oriented flush with respect to the bottom tunnel wall and one with its exit plane extending from the injection wall into the tunnel (figure 3). The nozzles were otherwise nearly identical in shape: they were formed with a fifth-order polynomial contraction, had an inner diameter at the

https://doi.org/10.1017/S0022112007008385 Published online by Cambridge University Press

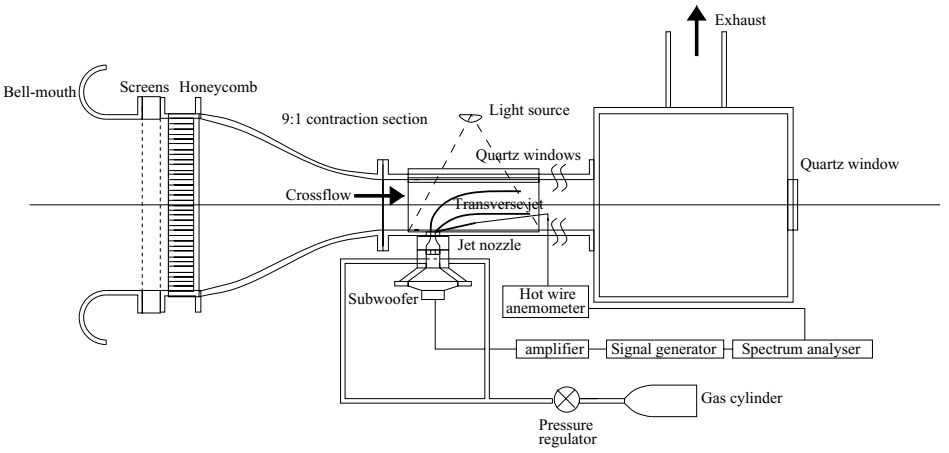


FIGURE 2. Schematic diagram of the low-speed wind tunnel and associated transverse-jet excitation apparatus (where excitation was used for only low-level forcing in the present experiments). The actual tunnel had three additional sections situated downstream of the one shown, of identical dimensions.

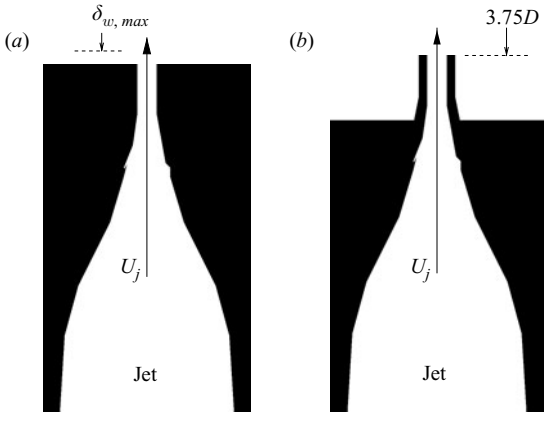


FIGURE 3. Schematic representations of the (*a*) flush and (*b*) elevated nozzles used in the present experiments. δ_{max} indicates the maximum relative size measured for the wall boundary-layer thickness. The exit for the elevated nozzle lay 3.75 diameters above the wind-tunnel lower wall.

nozzle exit of 3.81 mm, and had the same nozzle length and distance between the gas inlet and nozzle exit plane. The flush nozzle used in earlier experiments (M'Closkey *et al.* 2002; Shapiro *et al.* 2006) had a nozzle exit diameter twice as large as in the present experiments but still with a fifth-order polynomial contraction. Jet exit velocities ranging from $5\,\mathrm{m\,s^{-1}}$ to $20\,\mathrm{m\,s^{-1}}$ were explored; results for exit velocities of $8\,\mathrm{m\,s^{-1}}$ ($Re = 2000$) and $12\,\mathrm{m\,s^{-1}}$ ($Re = 3000$) were the focus of the detailed studies presented herein.

These nozzles were designed to achieve nearly top-hat velocity profiles at the exit plane, with a relatively small jet momentum thickness. In the absence of crossflow, the exit velocity profiles of the two nozzles were symmetric and virtually identical (see § 3.1). The exit plane of the elevated nozzle lay 14.3 mm (or 3.75 exit diameters) from the bottom of the wind-tunnel wall, so that the contraction continued within

https://doi.org/10.1017/S0022112007008385 Published online by Cambridge University Press

the tunnel (figure 3). The elevation isolated the jet exit flow from that of the tunnel wall boundary layer, which for all conditions explored was less than two jet diameters thick in the vicinity of the flush jet. Yet, as will be shown, the relative shortness of the elevated nozzle allowed for the generation of vertical flow near the exit, which had an influence on the shear-layer instabilities for very large crossflow velocities.

The jet nozzle assembly shown in figures 2 and 3 consisted of the interchangeable nozzle, a 10 cm long cylindrical pipe section with an inner diameter of 3 cm, a Plexiglas plenum housing a loudspeaker (used during low-level excitation experiments), and an interchangeable cylindrical aft section of the plenum with a 12.7 cm inner diameter. The jet fluid, industrial nitrogen gas from a pressurized tank, was fed to the nozzle assembly at the cylindrical pipe section through four symmetrically oriented inlets fed from a plastic tube. Nitrogen flowed into the nozzle at room temperature, which was verified at the jet exit using a Type B thermocouple.

A single-component hot-wire anemometer (Dantec 55P15) enabled measurement of the spatial variation of the jet exit velocity as well as measurement of the spectral character of the vertical disturbance velocity in the jet shear layer. The hot wire was connected to a Dantec Dynamics StreamLine 90N10 frame, with the probe attached to three Newport high-performance low-profile ball-bearing linear stages creating a triple-axis manual traversing platform. This allowed movement of the hot wire in all x, y and z directions with an accuracy of 1 μm (2.6×10^{-4} jet diameters). Hot-wire output signals were fed to a dynamic signal analyser (HP-35665A), allowing a frequency range of up to 25 kHz, and to a high-speed data-acquisition system to enable the acquisition of power spectra. The hot wire was calibrated in the wind tunnel with respect to the crossflow using a Dwyer Pitot probe and two Omega Engineering (PX653-03D5V and PX653-0.25D5V) differential pressure transducers.

3. Results

3.1. *Mean transverse jet characteristics*

The effect of jet and crossflow conditions on mean velocity profiles near the jet exit revealed relatively small differences between the two nozzle configurations. The vertical component of the velocity was measured at various x locations across the nozzle exit, as close as $z/D = 0.1$ from the exit plane (see figure 1 for the present coordinate system). Figure 4 shows sample mean velocity profiles near the jet exit for different jet-to-crossflow velocity ratios R at a jet Reynolds number of 2000. Results for the standard deviation of the fluctuations near the jet exit at the same conditions are also shown. Data for both flush and elevated nozzles are provided in these plots; virtually identical scaled velocity and standard deviation profiles were observed for these conditions, but at a higher jet Reynolds number ($Re = 3000$). Uncertainties in velocity magnitude were approximately 0.05 % at the higher speeds (above 10 m s^{-1}) and up to 1.2 % at the lower speeds (1 m s^{-1}).

In the absence of crossflow ($R \to \infty$, figure 4*a*), the velocity profiles and fluctuations near the exit plane were virtually symmetric, and were nearly the same for each nozzle and Reynolds number explored, since the area contractions in both flush and elevated nozzles were nearly identical. Small differences in machining the two nozzles probably produced the small differences in velocity profiles observed for the free jet, producing slightly different momentum thicknesses for the elevated nozzle as for the flush nozzle for most values of R, as indicated in table 2. Uncertainties in momentum thickness largely arose from the selection of the initial exterior point in the integration; for the flush jet, this uncertainty was as high as 7.8 %, whereas for the elevated jet it was smaller, of the order of 5.4 %.

https://doi.org/10.1017/S0022112007008385 Published online by Cambridge University Press

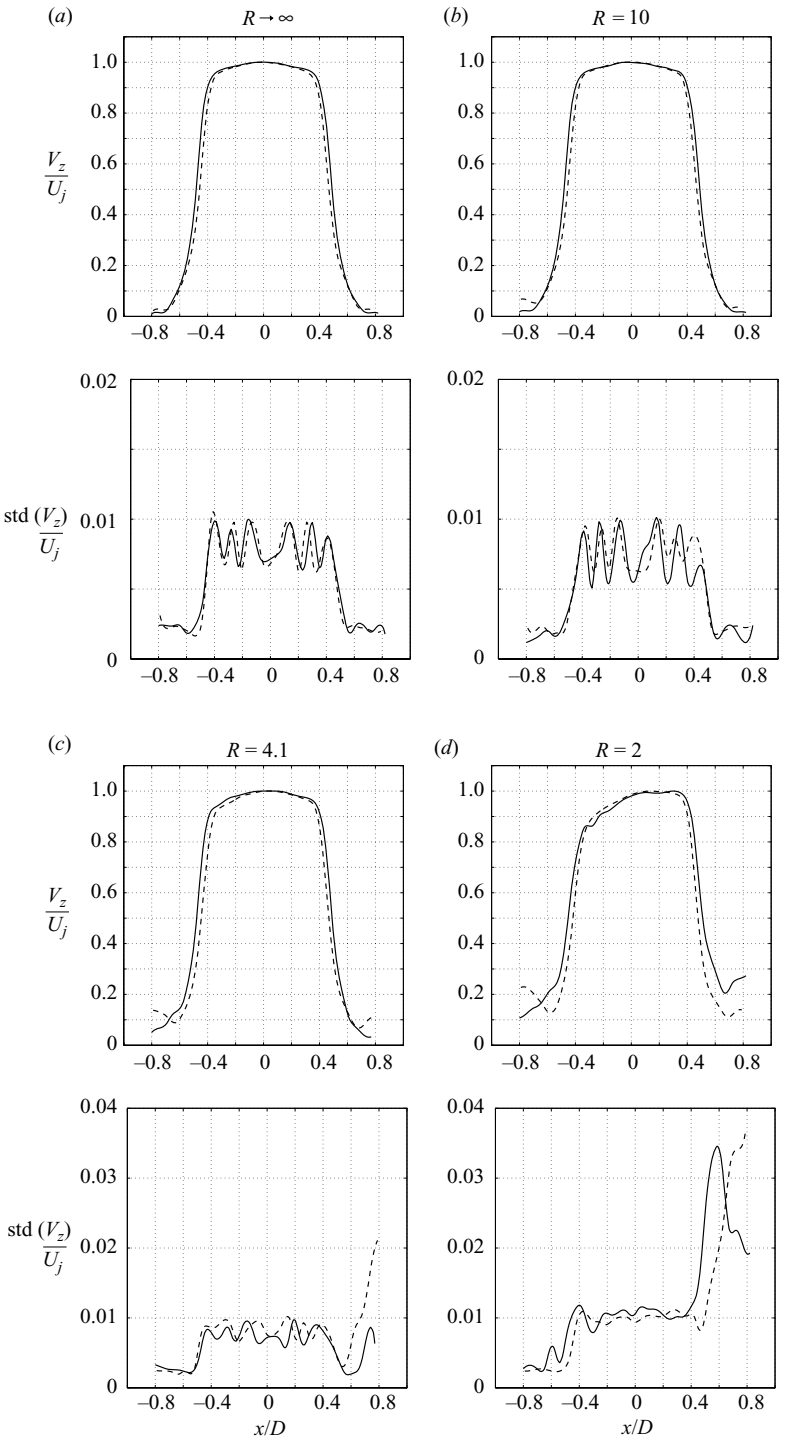


FIGURE 4. Velocity profiles (upper) and scaled values of the standard deviation of the fluctuating vertical velocity component (lower), measured at a location $z/D = 0.1$ above the exit plane, at $y = 0$. Results are given for the flush (solid line) and elevated (dashed line) nozzles at various jet-to-crossflow velocity ratios R. Conditions correspond to a jet Reynolds number of 2000.

https://doi.org/10.1017/S0022112007008385 Published online by Cambridge University Press

	Flush, $Re = 2000$		Elevated, $Re = 2000$		Flush, $Re = 3000$		Elevated, $Re = 3000$	
R	$\theta_{fl,u}/D$	$\theta_{fl,d}/D$	$\theta_{el,u}/D$	$\theta_{el,d}/D$	$\theta_{fl,u}/D$	$\theta_{fl,d}/D$	$\theta_{el,u}/D$	$\theta_{el,d}/D$
∞	0.051	0.052	0.053	0.053	0.046	0.046	0.048	0.048
10	0.053	0.053	0.053	0.053	0.047	0.047	0.050	0.049
8.0	0.055	0.055	0.053	0.053	0.049	0.047	0.053	0.048
7.8	0.054	0.054	0.053	0.053	0.050	0.047	0.053	0.049
6.4	0.056	0.052	0.054	0.053	0.053	0.049	0.053	0.049
6.0	0.056	0.052	0.054	0.054	0.054	0.048	0.050	0.047
5.2	0.058	0.052	0.055	0.054	0.057	0.050	0.052	0.048
4.1	0.065	0.052	0.057	0.054	0.064	0.050	0.053	0.048
3.0	0.076	0.053	0.060	0.052	0.076	0.053	0.061	0.051
2.0	0.103	0.057	0.066	0.053	0.110	0.059	0.062	0.052
1.5	0.109	0.062	0.076	0.053	–	–	–	–
1.2	0.113	0.062	0.097	0.054	–	–	–	–
1.15	0.117	0.067	0.106	0.053	–	–	–	–

TABLE 2. Upstream (subscript u) and downstream (subscript d) transverse-jet shear-layer momentum thicknesses measured at $z = 0.1D$ above the nozzle exit, for flush and elevated nozzles. Momentum thicknesses are scaled by jet diameter D and are given for different values of jet-to-crossflow velocity ratio R and for different jet Reynolds numbers.

As the crossflow was turned on so that U_∞ increased and R decreased for a fixed jet Reynolds number, there was initially no significant alteration in the jet profile near the nozzle exit, either for the flush or the elevated nozzles, until about $R = 4.1$ (see figure 4c). The elevated jet experienced a slightly greater deflection of the upstream shear layer than did the flush jet, consistent with the observations of Smith & Mungal (1998) and the effectively smaller crossflow seen by the flush jet owing to the influence of the wall boundary layer. At $R = 3$ and below, differences between flush and elevated jet profiles became more obvious, indicated, for example, in figure 4(d) for $R = 2$. There was evidence of positive vertical flow exterior to the elevated nozzle at this larger crossflow condition (for $x/D < -0.5$). The relatively large fluctuations at the downstream jet shear layer at these lower R values for both nozzles were consistent with the presence of vorticity generation via wake vortices associated with the wall boundary layer in the case of the flush injection or with the wake flow about the elevated nozzle.

In other experiments (Megerian & Karagozian 2005), for a fixed jet Reynolds number, the end of the potential core for the transverse jet was observed to lie closer to the jet exit than that of the free jet, consistent with the notion of increased near-field mixing by the transverse jet. The somewhat enhanced skewing of the jet's velocity profile at lower R values near the exit plane also indicated an increase in the jet momentum thickness at the upstream edge of the shear layer in comparison to its downstream jet momentum thickness (table 2).

For very low R values ($R < 3$), the flush jet's momentum thickness became larger than for the elevated jet under the same conditions. These differences in the exit profile between flush and elevated jets and among different ranges for R provide evidence that the transverse-jet shear-layer instability could be different for different operating conditions. As noted by Michalke (1971) and Kibens (1981) for the free jet and in Alves *et al.* (2007*b*) for the transverse jet, alteration in the jet momentum thickness with different flow conditions could result in a change in the frequency or Strouhal number as well as a change in the amplitude of the most unstable frequency.

It is of interest to quantify the flow field in the vicinity of (but exterior to) the elevated nozzle and its effect on the transverse-jet shear layer. Figure 5 shows the local

https://doi.org/10.1017/S0022112007008385 Published online by Cambridge University Press

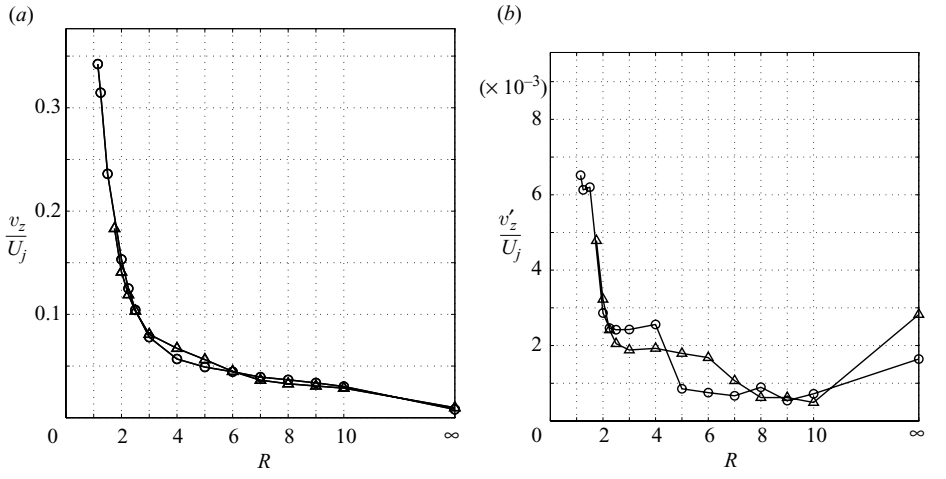


FIGURE 5. Plots of (*a*) vertical velocity component v_z and (*b*) standard deviation of the fluctuating velocity, each scaled by jet velocity, and measured at a point upstream of the elevated jet nozzle (at a location $x=-1.0D$, $y=0$, and $z=-0.1D$). Results are shown for different values of the jet-to-crossflow velocity ratio R and for two different jet Reynolds numbers: ○, 2000; △, 3000.

vertical velocity and velocity fluctuations exterior to the nozzle, just below the elevated nozzle exit plane, for both $Re=2000$ and 3000. The velocity measurements indicated that as the crossflow magnitude U_∞ was increased, the vertical velocity exterior to the elevated nozzle increased slightly, but remained below 5 % of the jet velocity magnitude until the crossflow-to-jet velocity ratio R fell below about 4.1. For $R=2$, the exterior velocity reached as high as 15 % of the jet velocity, for either jet Reynolds number. For the case of the lower Reynolds number, $Re=2000$, the external velocity became as high as 35 % of the mean jet speed for the strongly deflected transverse jet with $R=1.15$. At these lower R values, the fluctuations in vertical velocity within the shear layer also increased substantially, from 0.3 % for $R\geqslant 2$ to 0.65 % for $R=1.15$. For $R\leqslant 3$, then, the local flow was observed to have some characteristics of a 'coflowing' jet, with the external flow having a non-negligible component in the same direction as that of the exiting jet flow. The impact of uniform coflow on a circular jet's shear-layer instabilities has been explored in the past, for example, by Michalke & Hermann (1982). This theoretical study indicates that with increasing external flow, the jet flow becomes less (convectively) unstable, but the region of unstable frequencies increases. A coflow magnitude that is 25 % of the jet velocity, for instance, is shown to reduce the growth rates of both axisymmetric and azimuthal instabilities by nearly 40 %. The effect of the coflow on the elevated transverse jet's upstream shear-layer instabilities in the present experiments will be discussed below.

As noted previously, the tunnel-wall boundary layer remained less than two jet diameters in height ($\delta_{99\,\%}$) for the range of crossflow conditions explored. Table 3 shows approximate values of the momentum thicknesses for the wall boundary layer, θ_w, just upstream of the flush jet exit. Under all conditions explored, the elevated nozzle's exit plane lay well above the tunnel-wall boundary-layer region.

3.2. *Transverse jet upstream shear-layer instabilities*

This section will describe results for the evolution of the instabilities along the upstream shear layer of the transverse jet for various jet-to-crossflow velocity ratios, including $R\rightarrow\infty$, the free-jet limit. Trajectories of the upstream shear layer were

https://doi.org/10.1017/S0022112007008385 Published online by Cambridge University Press

Re_∞	2005	1680	1400	1280	900	480	330
θ_w/D	0.05	0.07	0.12	0.17	0.17	0.24	0.19

TABLE 3. Approximate values of scaled wall boundary-layer momentum thickness just upstream of the flush jet orifice, for different crossflow Reynolds numbers $Re_\infty \equiv DU_\infty/\nu$. Typical values of R range from the order of 1.0 for $Re_\infty = 2005$ to the order of 10 for $Re_\infty = 330$.

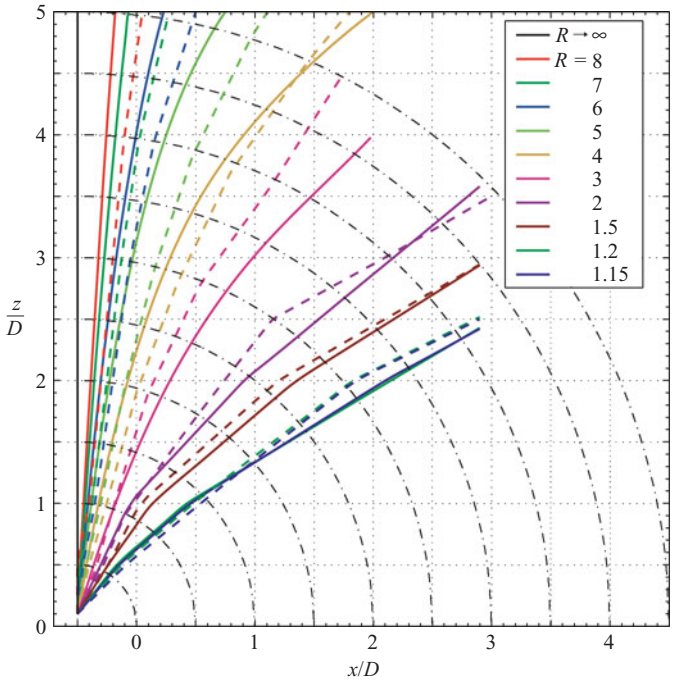


FIGURE 6. Near-field trajectories of the centre of the upstream shear layer for various jets in crossflow, for different jet-to-crossflow velocity ratios R. Solid lines correspond to trajectories for the flush jet and dashed lines are for the elevated jet trajectories. Data shown are for the $Re = 2000$ case.

determined from the loci of the local inflection point and the maxima in fluctuation amplitude within the velocity profile at locations above the jet exit. A plot of the upstream shear-layer trajectories in the near field of the jets, for both flush and elevated jets, is shown in figure 6 for $Re = 2000$, for example. For $R \geqslant 4$, the trajectory of the shear layer for the flush jet penetrated a little further (higher in z for a given x location) than for the elevated jet. This observation is consistent with the slight blockage (lower-speed local crossflow) that the wall boundary layer provides for the flush jet, allowing it to penetrate slightly more vertically than if there were full magnitude crossflow, as approximately seen by the elevated jet. For the cases where $R < 4$, however, the trend appeared to change, where the penetration of the elevated jet was actually greater than for the flush transverse jet. Under these conditions, the relative thinning of the wall boundary layer created a higher effective crossflow seen by the flush jet, allowing it to turn more significantly, whereas the increasing coflow exterior to the elevated nozzle at the same mean value of R actually deflected the effective crossflow, reducing its magnitude in the x-direction enough to allow the elevated transverse jet to penetrate a little further than the flush jet.

https://doi.org/10.1017/S0022112007008385 Published online by Cambridge University Press

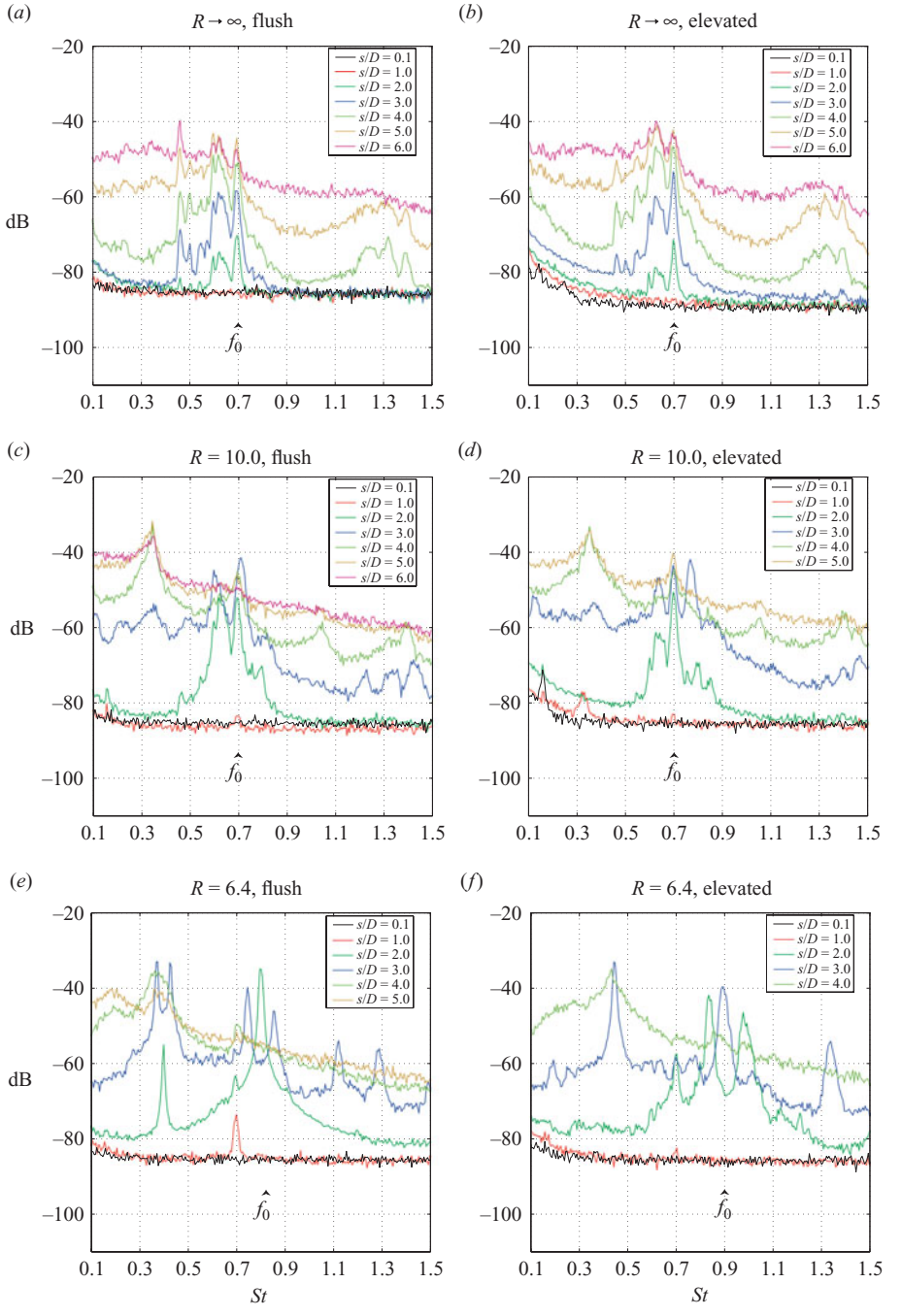


FIGURE 7. Vertical velocity spectra for the free (a, b) and transverse jet at various values of the jet-to-crossflow velocity ratio R, measured within the jet shear layer at different distances s from the jet exit. Results for both flush and elevated injection systems are shown. Conditions correspond to a jet Reynolds number of 3000.

Upon determination of the upstream shear-layer trajectories as shown in figure 6, spectra for the vertical velocity component were then acquired along the shear-layer trajectory. These spectra are shown in figures 7 and 8 for $Re = 3000$ and in figures 9, 10, and 11 for $Re = 2000$.

https://doi.org/10.1017/S0022112007008385 Published online by Cambridge University Press

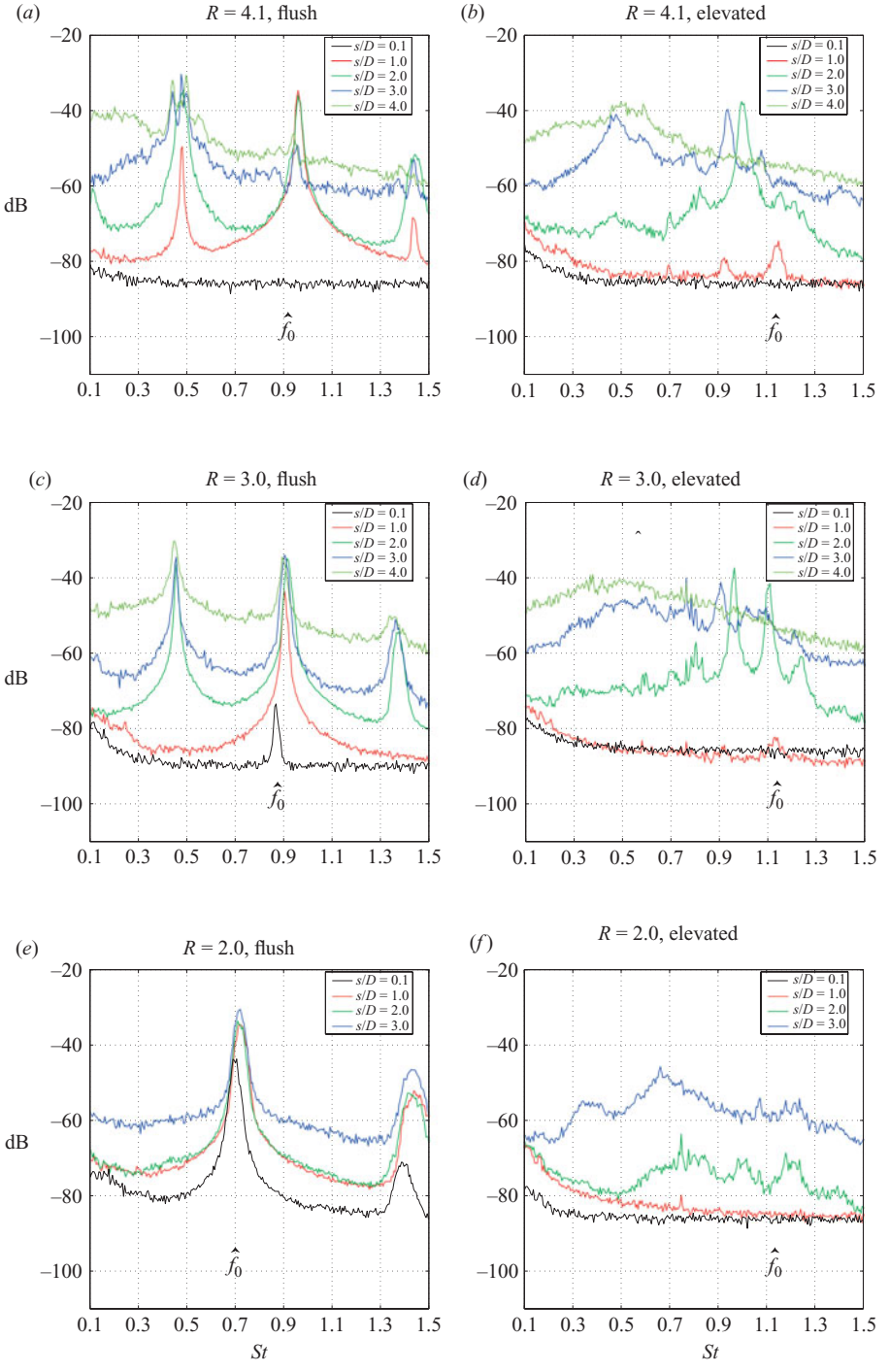


FIGURE 8. Vertical velocity spectra for the transverse jet at moderately low values of the jet-to-crossflow velocity ratio R, measured within the jet shear layer at different distances s from the jet exit. Results for both flush and elevated injection systems are shown. Conditions correspond to a jet Reynolds number of 3000.

https://doi.org/10.1017/S0022112007008385 Published online by Cambridge University Press

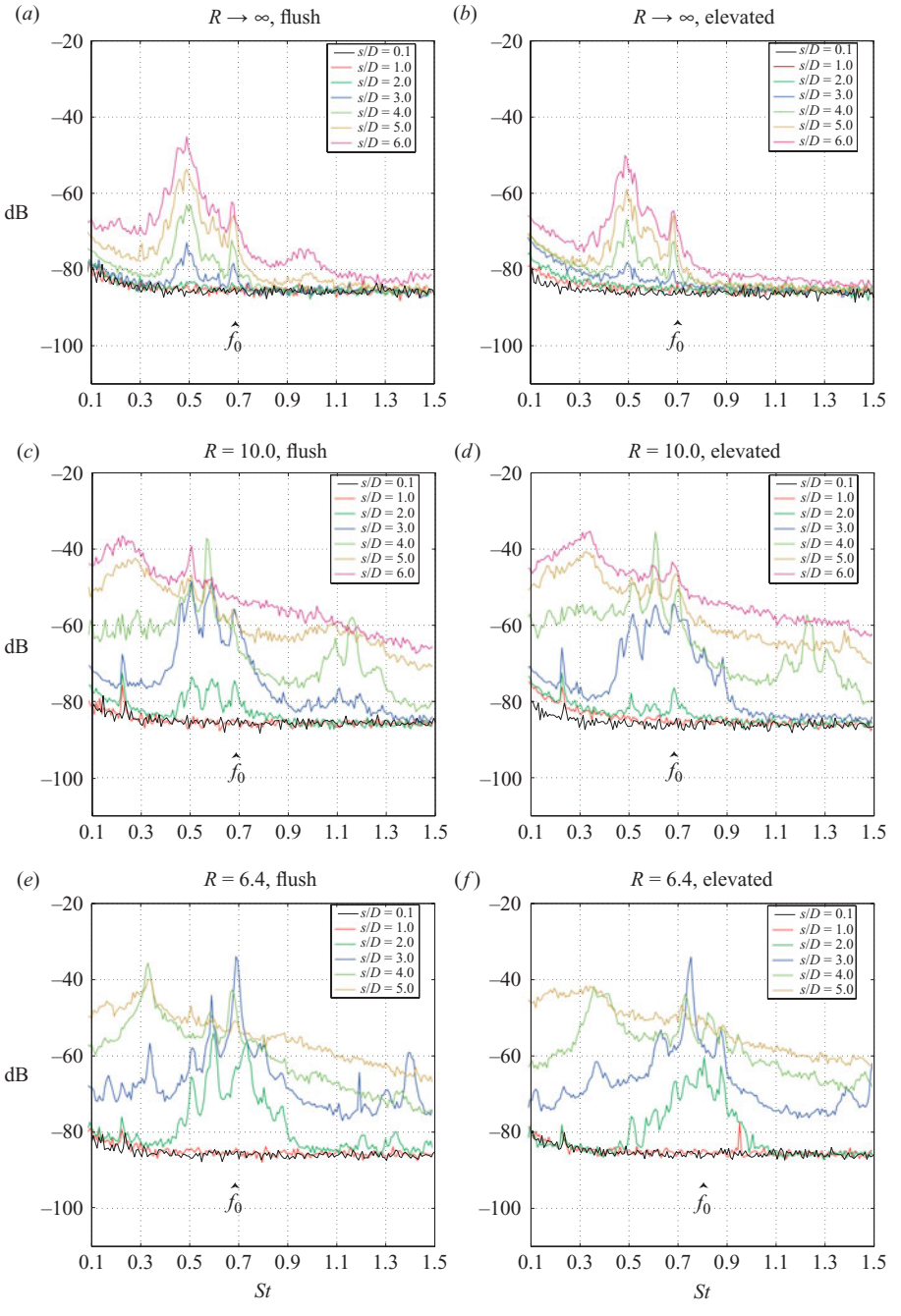


FIGURE 9. As for figure 7, but for a jet Reynolds number of 2000.

For laminar and transitional conditions at the jet exit, the spatial evolution of the free jet's shear-layer instability was found to be consistent with those documented in the literature (e.g. Petersen & Samet 1988; Xu & Antonia 2002). Results for the vertical velocity spectra, measured along the free jet's shear layer starting at a location $s/D = 0.1$, are shown for example in figures 7(*a*) and 7(*b*) for the flush and elevated

https://doi.org/10.1017/S0022112007008385 Published online by Cambridge University Press

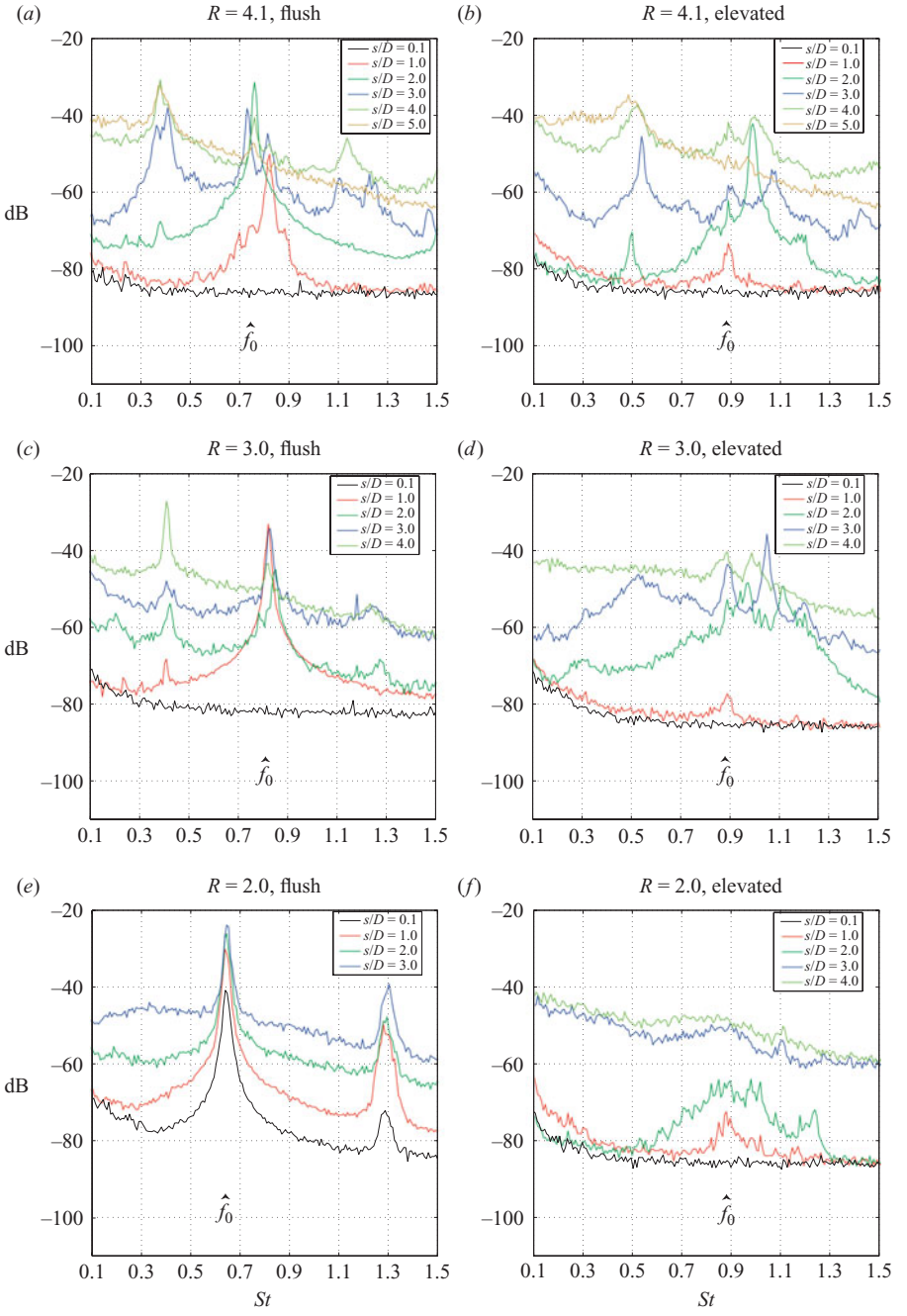


FIGURE 10. As for figure 8, but for a jet Reynolds number of 2000.

nozzles, respectively, at a Reynolds number of 3000. Here, s is the distance along the shear layer measured from the jet exit. We can see the initial growth of a spectral peak near a Strouhal number of 0.7, typically called the early 'shear-layer mode'. A slightly lower frequency near $St = 0.5$ also was initiated near the exit plane, eventually becoming more dominant downstream as the jet's 'preferred mode'. Similar spectral

https://doi.org/10.1017/S0022112007008385 Published online by Cambridge University Press

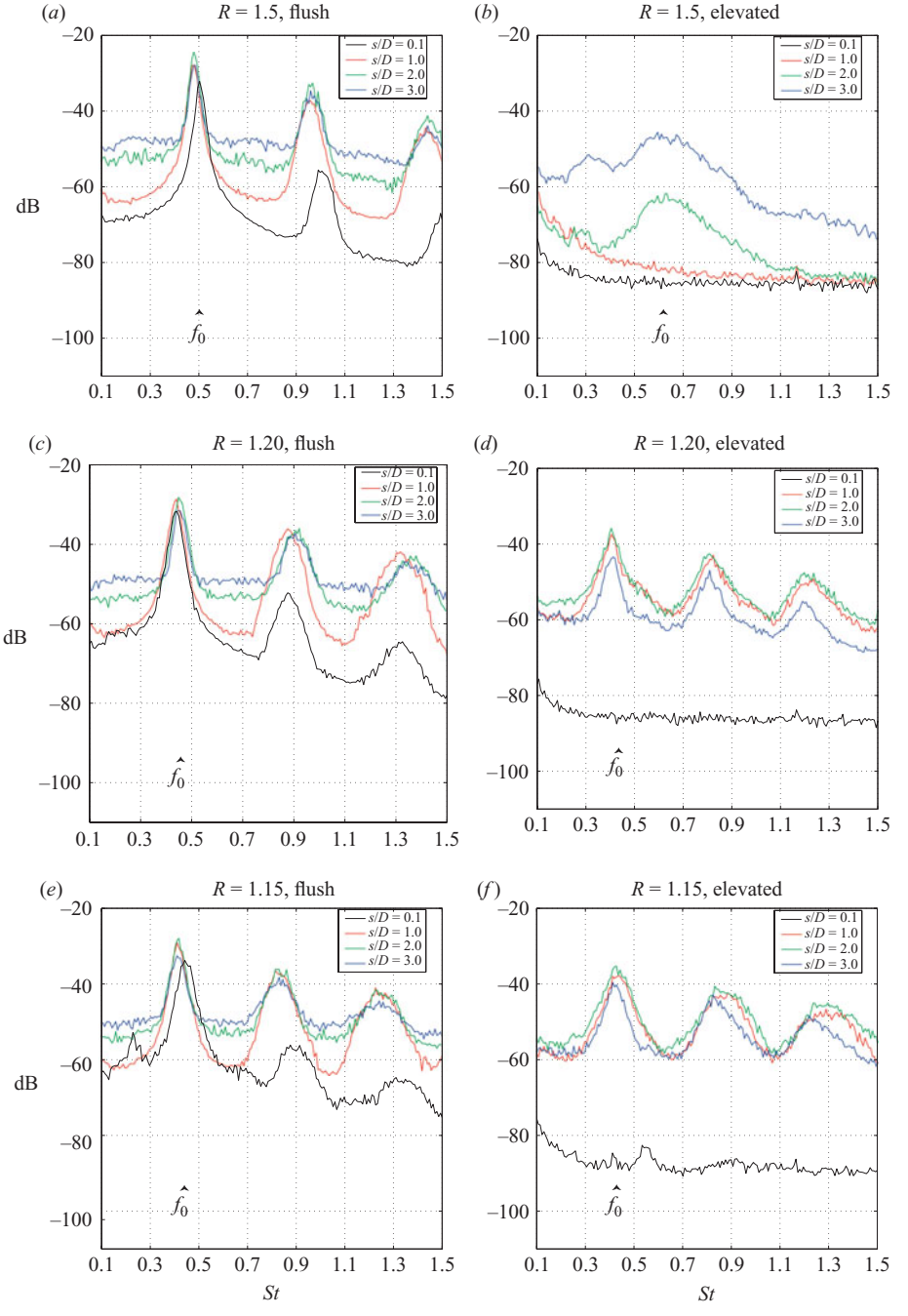


FIGURE 11. Vertical velocity spectra for the transverse jet at very low values of the jet-to-crossflow velocity ratio R, measured within the jet shear layer at different distances s from the jet exit. Results for both flush and elevated injection systems are shown. Conditions correspond to a jet Reynolds number of 2000.

evolution was found for the free jet with $Re = 2000$ (figures 9*a*, *b*). These spectra are similar to those observed by Xu & Antonia (2002) for the free jet with a near-top-hat velocity profile at the jet exit, but at a much higher Reynolds number (86 000). Weak

https://doi.org/10.1017/S0022112007008385 Published online by Cambridge University Press

harmonics above $St = 1.0$ were also observed, for both flush and elevated nozzles, but these were relatively weakened with downstream distance along the jet shear layer. This type of spectral character was regarded to be the free-jet 'baseline' against which the effect of increasing the crossflow velocity was compared.

For a fixed jet velocity, as the crossflow velocity was increased from zero, the spectral character of the jet shear layer changed in a number of ways. Spectral measurements made in the regime of relatively high R values ($R = 10,\ 6.4$) are shown in figures 7(c–f) for $Re = 3000$ and 9(c–f) for $Re = 2000$, for both flush and elevated transverse jets. Multiple modes or peaks in the range of Strouhal numbers between 0.5 and 0.7 were initiated, appearing successively closer to the jet exit as the crossflow velocity was increased. As we move along the upstream shear layer, the amplitude of one of the peaks was observed to increase, with a slight reduction in the frequency of the mode before being overtaken subsequently along the jet by a slightly higher-frequency mode. This behaviour will be further discussed later in connection with contour plots of these data. There was also the development of higher harmonics, indicating the initiation of nonlinear behaviour, and subharmonics, indicating pairing of vortical structures. The strength of the dominant modes also appeared to increase with decreasing values of R, or higher crossflow velocity, for both the flush and the elevated-jet nozzle in this range of R.

When the jet-to-crossflow velocity ratio R was reduced below about 3.5 to 4, however, the behaviour of the two different jet shear layers began to diverge. For $R < 3.5$, the flush jet dramatically transitioned in its spectral character, exhibiting a strong distinct fundamental mode very close to the jet exit. For example, results for flush jets with $4.1 \geqslant R \geqslant 2$ are shown in figures 8(a, c, e) for $Re = 3000$ and in figures 10(a, c, e) for $Re = 2000$. This remarkably strong instability was observed to occur very close to the jet exit for both $R = 3$ and $R = 2$, for both Reynolds numbers. For flush jets at $R = 3$, there was the appearance of a subharmonic and a higher harmonic further downstream, whereas only the higher harmonic appeared for $R \leqslant 2$. The rapid initiation of a strong dominant mode and harmonics with the increase in the crossflow magnitude for the transverse jet appeared to be qualitatively similar to spectral characteristics observed in the heated free jet beyond a critical density ratio (Monkewitz *et al.* 1990) or to spectra for the circular jet with counterflow beyond a critical magnitude (Strykowski & Niccum 1991). Each of these other configurations is associated with a transition from convective to absolute instability. The transition in the character of the velocity spectra is evidence of limit-cycle behaviour, which can suggest the presence of a globally unstable mode. Further exploration of this transition will be discussed in § 3.3.

In the present experiments, for $4.1 \geqslant R \geqslant 2$, the elevated jet in crossflow underwent a transition, evolving from spectra which were similar to the flush jets at $R = 4.1$ to spectra that were somewhat weaker as R was reduced. At $R = 2$ for the elevated nozzle, for example, shown in figure 8(f) for $Re = 3000$ and in figure 10(f) for $Re = 2000$, the instability appeared to be significantly diminished overall in strength, with much broader peaks.

For the jets with $Re = 2000$, the crossflow magnitude could be increased even further than that shown in figure 10, producing R values as small as 1.15. The spectra for $Re = 2000$ in the range $1.5 \geqslant R \geqslant 1.15$ are shown in figure 11. When R was reduced to 1.5 and 1.25 (not shown), the flush jet continued to exhibit strong modes with initial frequencies near $St = 0.5$, with additional strong harmonics generated close to the jet exit. For these R values, the elevated jet continued to exhibit weakened instabilities with broader peaks. However, when R was reduced below 1.25, to 1.20

https://doi.org/10.1017/S0022112007008385 Published online by Cambridge University Press

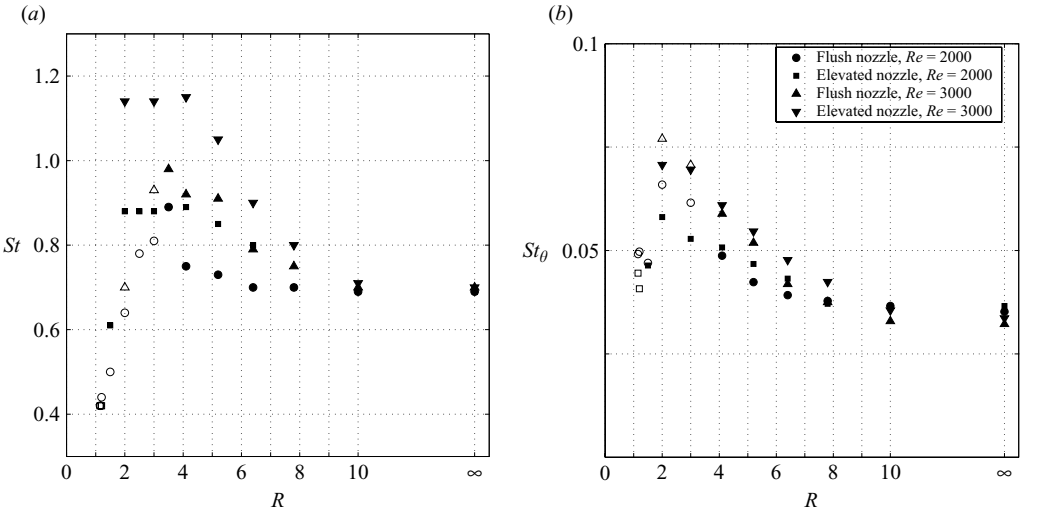


FIGURE 12. (*a*) Variation in the Strouhal number (based on D) associated with f_0, the frequency of the dominant instability first observed to occur along the upstream jet shear layer, for different values of the jet-to-crossflow velocity ratio R. (*b*) The same data, but plotted in terms of a Strouhal number based on upstream momentum thickness, St_θ. Results for both jet Reynolds numbers are shown, and for both elevated and flush injection. The open symbols represent dominant Strouhal numbers associated with very strong instabilities generated very close to the jet exit.

and 1.15, the elevated jet's shear layer exhibited a remarkable transition from weak, diffuse peaks to stronger, distinctive modes (shown in figures 11*d*, *f*). These stronger modes were qualitatively and quantitatively similar to those generated by the flush nozzle at $R = 1.20$ and 1.15, generating modes with initial St near 0.4, as indicated in figures 11(*c*, *e*). After a rapid turning of the transverse jet at such low jet-to-crossflow velocity ratios, the elevated jet's shear layer appeared to become very much like that of the flush-injected jet. The very weak disturbance at $St \approx 0.52$, observed close to the nozzle exit for the elevated jet at $R = 1.15$ (see figure 11*f* at $s/D = 0.1$), died out quickly along the jet shear layer. A weak disturbance at this frequency was also detected upstream of the elevated jet's nozzle under these conditions, and hence the disturbance was probably related to the upstream flow conditions and not to the jet shear layer itself.

Spectral results in figures 7 to 11 also identify the Strouhal number associated with f_0, the frequency of the initial fundamental instability mode that was observed to develop along the jet shear layer. Strouhal numbers associated with f_0 at higher values of R (above about 4 or 5) are probably a quantification of an early-developing 'shear-layer mode' rather than the ultimately dominant 'preferred mode' occurring further downstream, both of which are usually found in free jets (Petersen & Samet 1988). A plot of the Strouhal numbers (based on jet diameter D) corresponding to f_0 for different experimental conditions, i.e., jet Reynolds numbers and jet-to-crossflow velocity ratios R, is shown in figure 12a. The current configuration was such that the jets with $Re = 2000$ could achieve lower R values than those possible for $Re = 3000$, hence data for $R < 2$ appear only for $Re = 2000$. At the lower values of R (below 3.5 for the flush jet and below 1.25 for the elevated jet), f_0 represents the frequency of the very strong dominant mode that appeared to grow almost immediately downstream of the jet exit; these data are shown as open symbols in figure 12(*a*), in contrast to

https://doi.org/10.1017/S0022112007008385 Published online by Cambridge University Press

the filled symbols for the somewhat weaker, spatially evolving instabilities at higher R values. Figure 12(b) shows the same data, but with Strouhal number scaled with respect to the initial upstream jet momentum thickness, so that $St_\theta = f_0\theta_{fl,u}/U_j$ for the flush jet and $St_\theta = f_0\theta_{el,u}/U_j$ for the elevated jet.

As the crossflow velocity U_∞ increased from zero, for the range $\infty > R > 8$, the dominant Strouhal number (either St or St_θ) did not change significantly for any of the test cases, remaining at approximately $St \approx 0.7$ ($St_\theta \approx 0.04$) for both Reynolds numbers. We note in the case of the free jet ($R \to \infty$) that an instability near $St = 0.5$ was also initiated relatively close to the exit plane for either jet configuration and for both Reynolds numbers, but was initially somewhat weaker than the $St \approx 0.7$ mode. This mode near $St = 0.5$ is not shown in figure 12(a, b), but did tend to grow stronger than the higher-frequency mode did in the downstream region of the shear layer, consistent with the behaviour of the commonly observed 'preferred mode' of the free jet.

As the crossflow velocity was increased and R decreased, the frequency of the initial disturbance f_0 began to increase for both nozzles and Reynolds numbers. Differences in the degree of increase in the Strouhal numbers with decreasing R among the cases shown were due at least in part to differences in the upstream shear-layer velocity profiles. When the initial frequency is scaled with respect to the upstream shear layer's initial momentum thickness (as done in figure 12b), the data collapse much better onto similar curves, with small differences based on Reynolds number. The systematic increase in the initial Strouhal number (as well as in the average of the frequencies that became dominant downstream) with decreasing R, observed for both nozzles and both Reynolds numbers, is predicted for the transverse jet's axisymmetric shear-layer mode by a local stability analysis at jet-to-crossflow velocity ratios in this range (see Part 2, Alves *et al.* 2007*b*).

For values of R below about 3.5, the trends in St begin to diverge. For the elevated jet, the value of St remained nearly constant for the range $4 \geqslant R \geqslant 2$ for either Reynolds-number condition (figure 12a). These frequencies were associated with the weakened instabilities observed in figures 8(d, f), 10(d, f), and 11(b) and were consistent with the increasing influence of the exterior coflow magnitude at higher crossflow velocities, at least, until $R = 1.2$ at $Re = 2000$. In figure 12(b), the elevated nozzle's scaled value of St_θ continued to increase for $4 \geqslant R \geqslant 2$, but to a much lesser extent than for the flush jet. In contrast, when the strong single modes (and harmonics) began to appear for $R \lesssim 3.5$ in the flush jet, the initial (and dominant) frequency began to drop off significantly with decreasing R values. This transition in the behaviour of the Strouhal number may have been related in part to increases in the jets' upstream shear-layer thicknesses at lower R values, since the increase in St_θ with decreasing R (figure 12b) continued until $R \approx 2$. The significant alteration in the spectral character of the shear layer under these conditions (as seen in figures 8c, e, 10c, e, and 11a, c–f) probably played a greater role in this rather dramatic change in frequency. Yet even the relatively weak instability associated with the elevated nozzle at $Re = 2000$ and $R = 1.5$ experienced a decline in the magnitude of St, so the association with the strong nonlinear shear-layer behaviour was not always observed.

Results such as those in figures 7 to 11 may be visualized more clearly using contour plots indicating the magnitude of the local instability at various non-dimensional downstream locations s/D associated with the frequencies of the instabilities, represented in terms of Strouhal number. Sample contour plots for both nozzles with $Re = 3000$ are shown in figures 13 and 14, corresponding to the spectra shown in figures 7 and 8, respectively. Contour plots for both nozzles with $Re = 2000$ are

https://doi.org/10.1017/S0022112007008385 Published online by Cambridge University Press

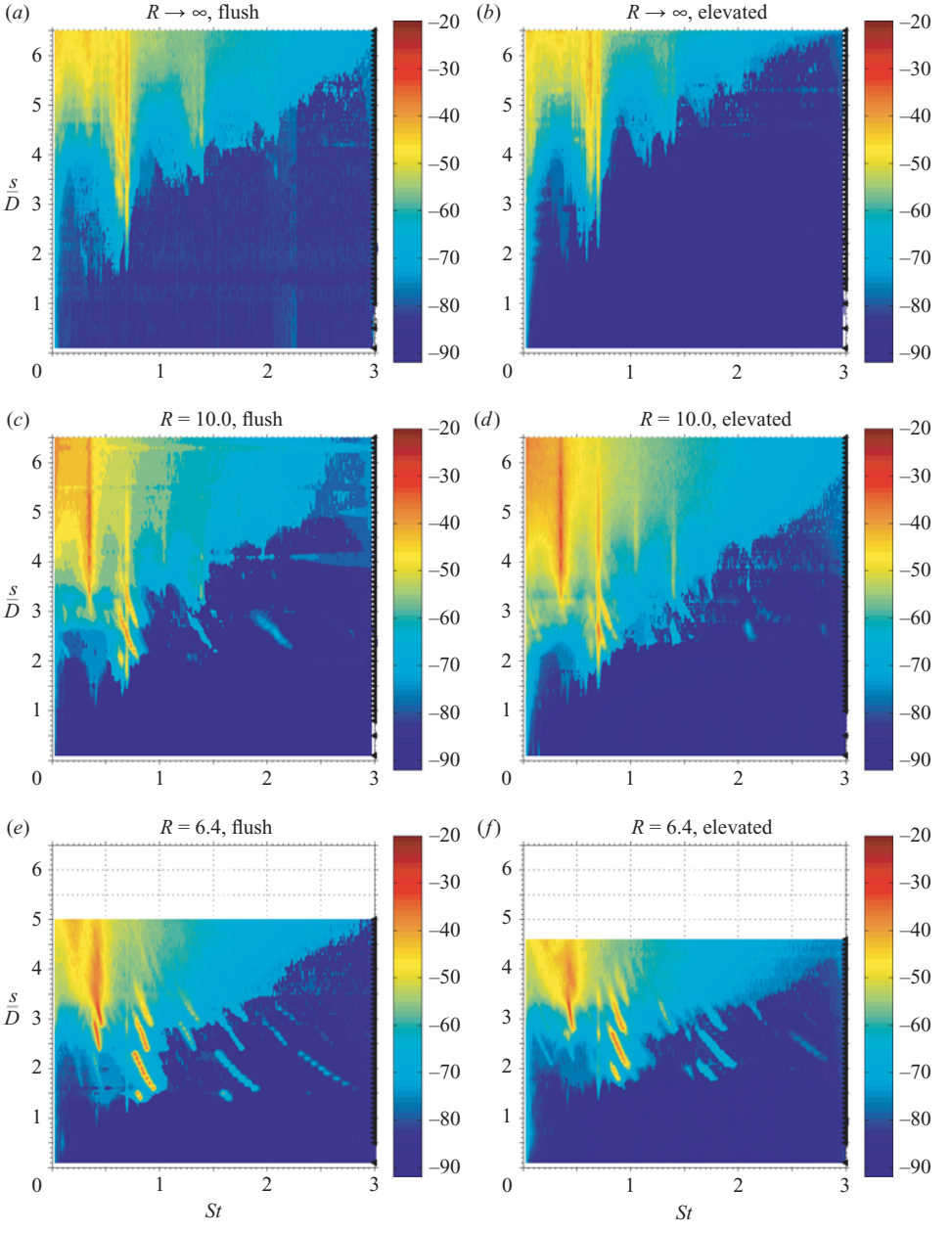


FIGURE 13. Contour plots of the amplitude and frequency (Strouhal number) associated with shear-layer instabilities occurring at various locations s/D along the transverse jet. Results are shown for the free (a, b) and transverse jet at various values of the jet-to-crossflow velocity ratio R. Amplitude *vs.* Strouhal number for both flush and elevated injection systems is shown. Conditions correspond to a jet Reynolds number of 3000.

shown in figures 15, 16 and 17, corresponding to the spectra in different R regimes shown in figures 9, 10 and 11, respectively.

Spectral differences between flush and elevated jets were made very clear in contour maps for the same values of R. The free jets for both nozzles exhibited the development

https://doi.org/10.1017/S0022112007008385 Published online by Cambridge University Press

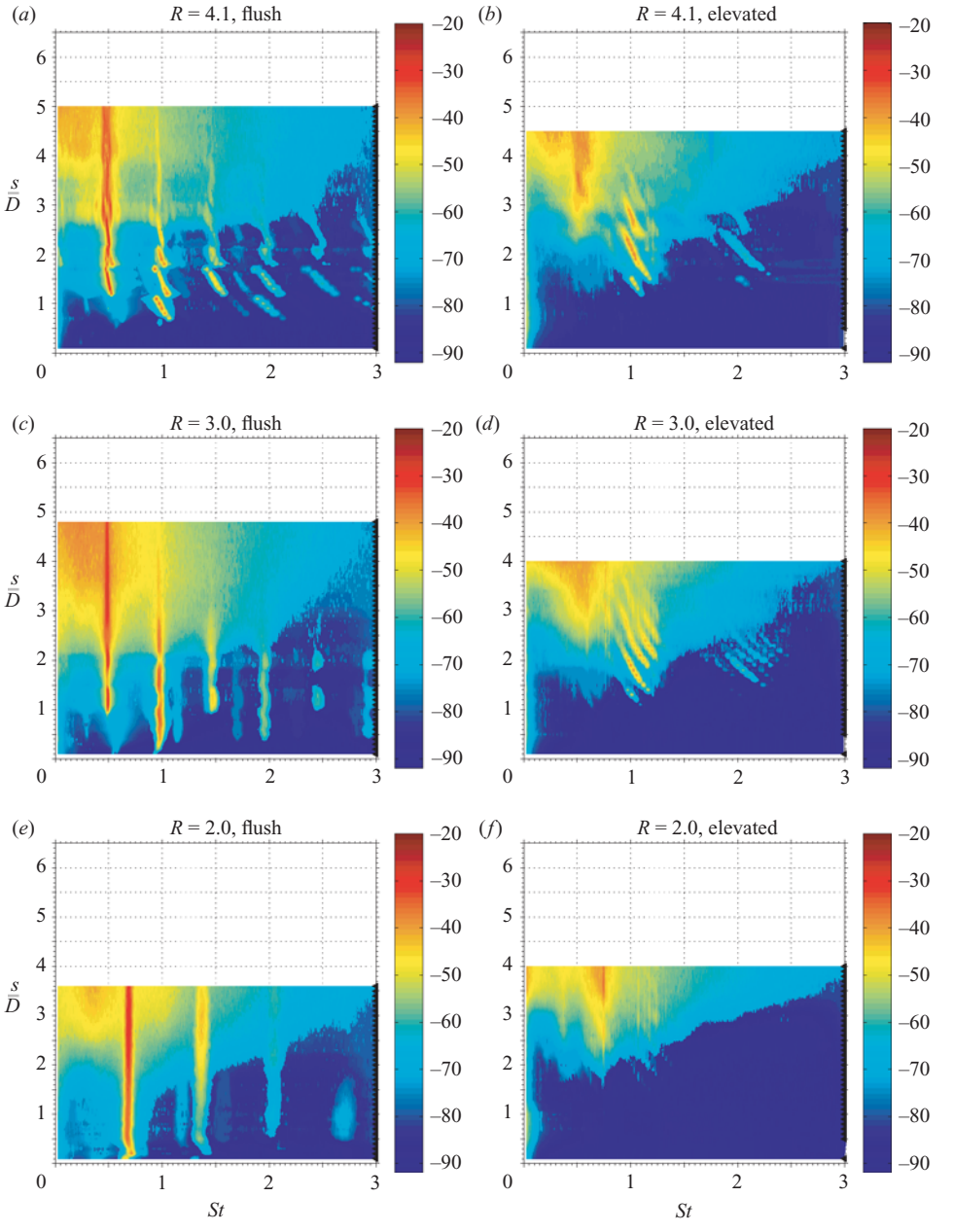


FIGURE 14. Contour plots of the amplitude and frequency (Strouhal number) associated with shear-layer instabilities occurring at various locations s/D along the transverse jet. Results are shown for the transverse jet at moderately low values of the jet-to-crossflow velocity ratio R. Results for both flush and elevated injection systems are shown. Conditions correspond to a jet Reynolds number of 3000.

of a relatively weak instability that was initiated over two diameters downstream of the jet exit for the lower Reynolds number (figure 15*a*, *b*) and just beyond one diameter downstream of the higher Reynolds number's jet exit (figure 13*a*, *b*).

https://doi.org/10.1017/S0022112007008385 Published online by Cambridge University Press

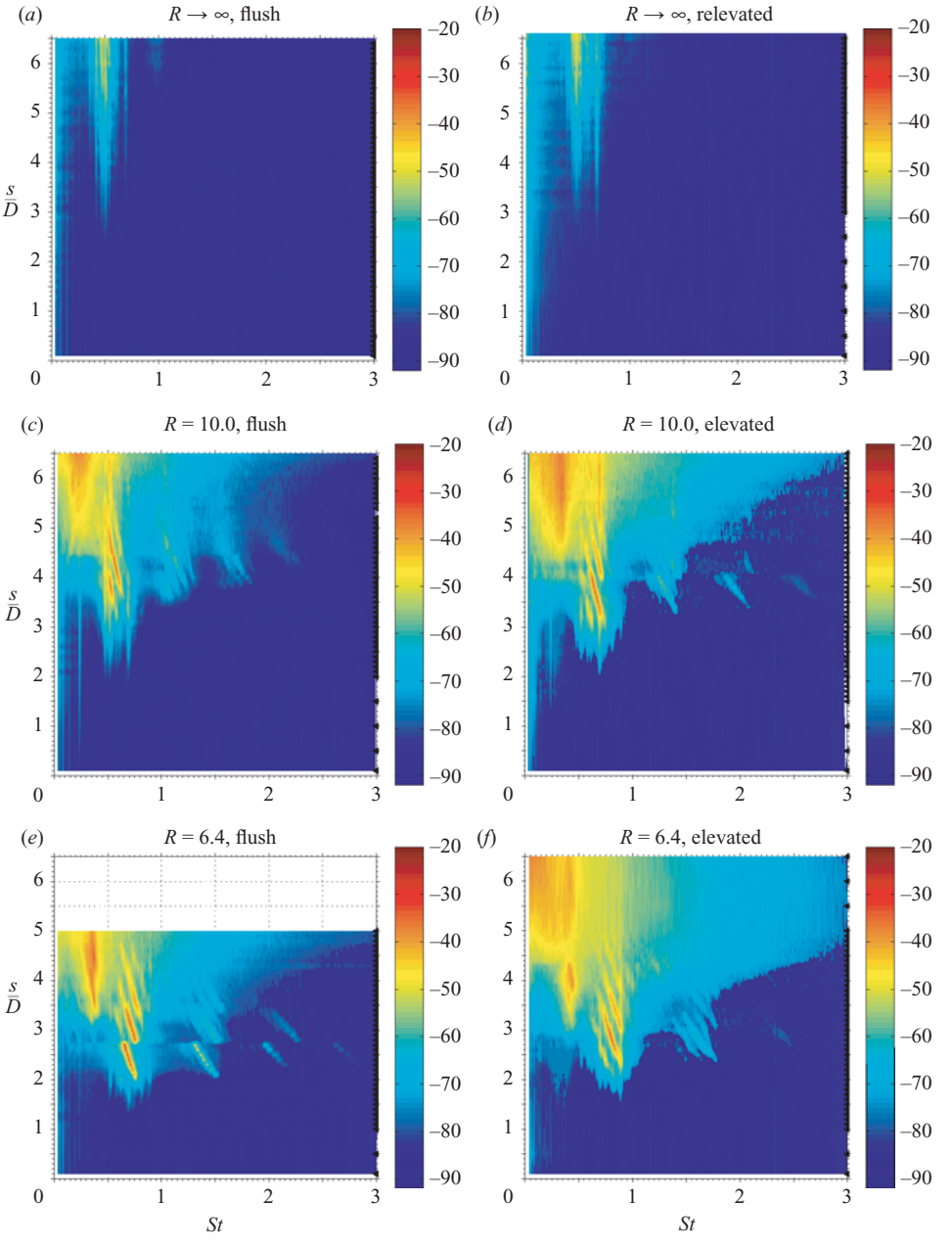


FIGURE 15. As figure 13, but for a jet Reynolds number of 2000.

When the crossflow was turned on, for $R = 10$ and 6.4, for example, the instabilities exhibited remarkably similar transitions (for both nozzles and for both Reynolds numbers), and these transitions distinctly marked the behaviour of the transverse jet as compared with the free jet. As shown in figures 13(c, d) and 15(c, d) for $R = 10$ and in figures 13(e, f) and 15(e, f) for $R = 6.4$, as the crossflow velocity was increased, the initiation of the instability occurred closer to the jet exit. Along the shear-layer the instability underwent a gradual drop in dominant frequency or Strouhal number,

https://doi.org/10.1017/S0022112007008385 Published online by Cambridge University Press

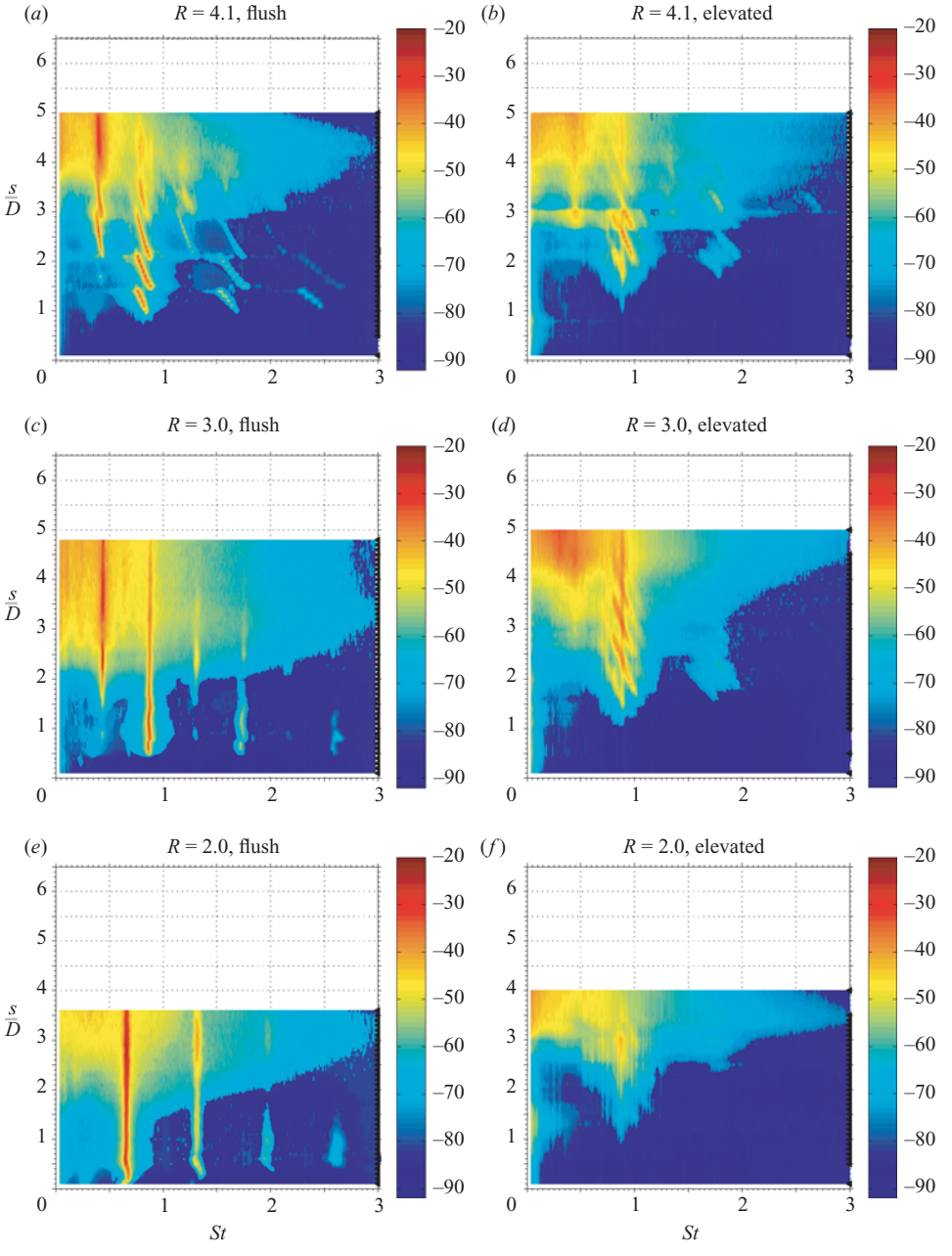


FIGURE 16. As figure 14, but for a jet Reynolds number of 2000.

then a sudden mode shift to a higher frequency, then a gradual reduction, then another jump to a higher frequency, in some cases repeating several times within 5–6 jet diameters from the orifice. Hence, the 2–3 peaks often observed in shear-layer spectra at a given s/D location, e.g. in figure 9(e, f), appeared to be related to a mode locking and switching phenomenon when examined in the contour plots, e.g. in figure 15(e, f). Nearly simultaneously, weaker harmonics of the fundamental mode(s) were formed, with the same mode-shifting behaviour as in the initial dominant mode.

https://doi.org/10.1017/S0022112007008385 Published online by Cambridge University Press

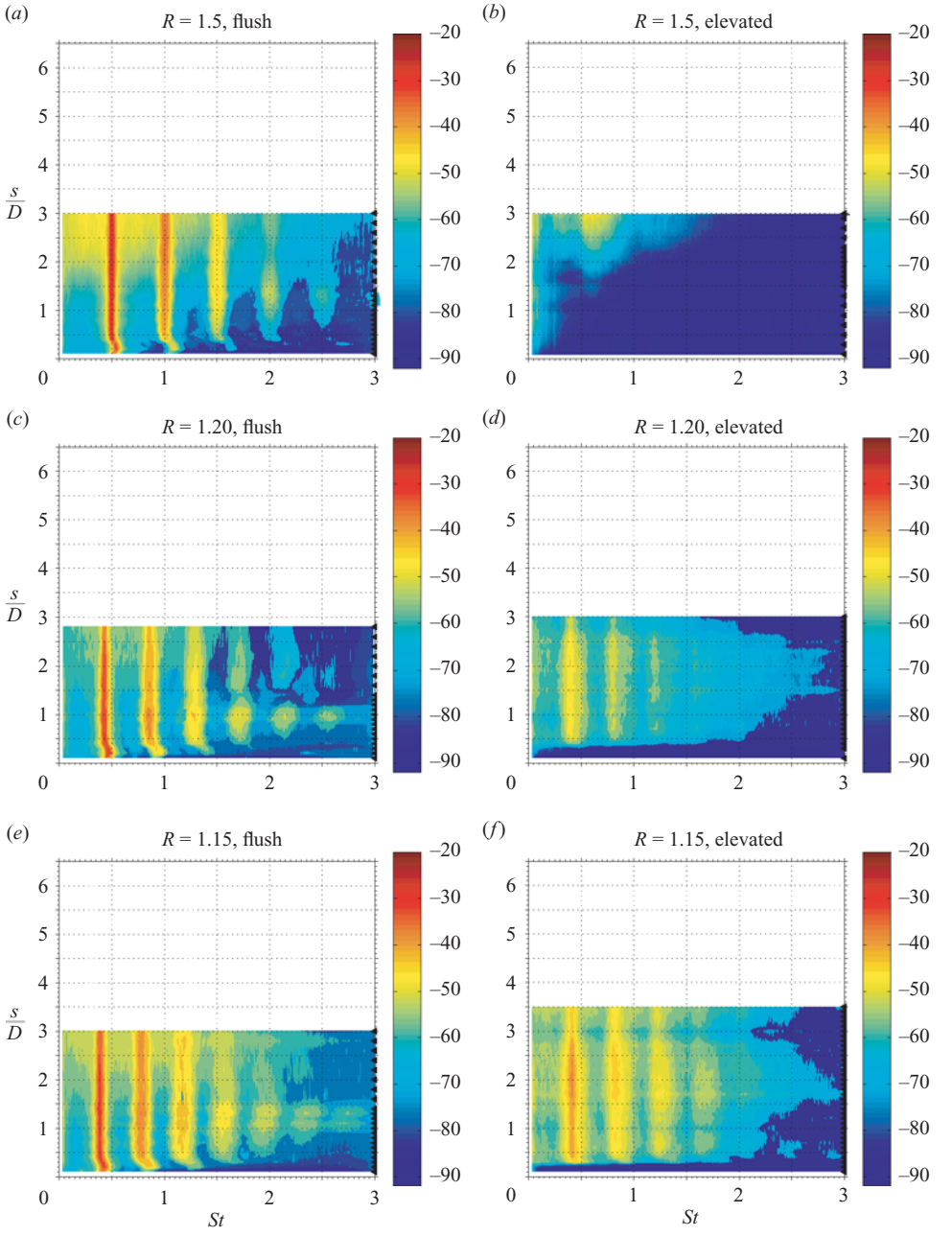


FIGURE 17. Contour plots of the amplitude and frequency (Strouhal number) associated with shear-layer instabilities occurring at various locations s/D along the transverse jet. Results are shown for the transverse jet at very low values of the jet-to-crossflow velocity ratio R. Results for both flush and elevated injection systems are shown. Conditions correspond to a jet Reynolds number of 2000.

Further downstream, high-amplitude subharmonics were formed for transverse jets in this regime, with somewhat similar mode-shifting behaviour as to that of the fundamental. This mode-shifting behaviour was observed for both flush and elevated nozzles, and for both Reynolds numbers in this moderate range of R values.

https://doi.org/10.1017/S0022112007008385 Published online by Cambridge University Press

When the jet-to-crossflow velocity ratio R was reduced below 3.5, as already noted by the spectra in figures 8 and 10, there was evidence in the flush jet of the generation of a strong distinct fundamental mode close to the jet exit, typically with rapid evolution of higher harmonics and subharmonics. This phenomenon is also exhibited in the contour plots in figures 14(a, c, e) and 16(a, c, e) for the two different Reynolds numbers in the range $4.1 \geqslant R \geqslant 2$. As the crossflow increased in magnitude, this remarkably strong instability was observed to occur closer to the flush jet exit, with a reduction in the initially dominant mode and, in the case of $R = 2$, disappearance of the subharmonic. No such transition in the instability for $4.1 \geqslant R \geqslant 2$ was observed for the transverse jet injected from the elevated nozzle (i.e. in figures 14b, d, f and 16b, d, f). In fact, as noted for the spectra, contour plots show that with increasing crossflow velocities in this range of R values, the elevated jet instabilities appeared to diminish in strength.

Figure 17 shows contour characterizations for a Reynolds number of 2000 for both nozzles at very low values of R (1.50, 1.20 and 1.15), corresponding to the spectra shown in figure 11. Although the instabilities for the elevated nozzle remained weak as the crossflow was increased for the range $2.0 \geqslant R \geqslant 1.25$, the increasing crossflow did cause the weak instability to be initiated closer to the jet exit in this range. When the crossflow was increased even further in magnitude, for $R \leqslant 1.2$, an initiation of stronger distinct modes (including the initiation of harmonics) similar to those seen for flush injection was observed (cf. figures 17d, f with 11d, f for the elevated jet and figures 17c, e with 11c, e for the flush jet). In the case of the flush nozzle, a continued strengthening of the strong dominant modes and harmonics, occurring even closer to the jet exit, were observed as R was reduced below 2.0.

To our knowledge, no such transitional behaviour in the nature of the upstream shear-layer instability has heretofore been documented quantitatively for the transverse jet, despite the robustness of the instability features such as mode shifting for the different injection and flow conditions. The significant alteration in the flush transverse-jet spectra as R was reduced below 3.5, and for the elevated-jet spectra for $R \leqslant 1.20$, may be related to the 'waving of the jet flow' observed by Camussi *et al.* (2002) in this regime. The present observations may relate to a coupling of the instability to the strong 'hovering vortex structure' that wraps around the front and sides of the jet, as indicated by Kelso *et al.* (1996) for relatively low R values and in the present study's Reynolds-number range. These authors suggest that the hovering vortex acts away from the jet orifice and is associated with the transverse jet itself. Clearly, the differences between the jet shear-layer instabilities for the flush- and elevated-nozzle cases in the $3.5 \geqslant R \geqslant 1.25$ range were due, at least in part, to the higher relative coflow present outside and upstream of the elevated nozzle (see figure 5a, b), which could be as high as 15 % of the mean jet velocity at R values near 2 and as high as 35 % for $R = 1.15$. This increased coflow appeared to have a stabilizing influence on the elevated-jet shear layer for $3.5 \geqslant R \geqslant 1.25$, consistent with the observations of Michalke & Hermann (1982) for coflowing jets undergoing convective instabilities. The flush-injected jet did not have such positive coflow; in fact, the presence of the horseshoe vortex as well as the 'hovering' vortex identified by Kelso *et al.* (1996) is thought to create a counterflow in the vicinity of the jet's upstream shear layer.

For $R \leqslant 1.25$, however, the elevated jet's shear-layer instability began to increase in magnitude, appearing similar to flush jet spectra (cf. figures 17c, d and 17e, f). While the exterior coflow continued to increase in this R regime, the elevated transverse

https://doi.org/10.1017/S0022112007008385 Published online by Cambridge University Press

jet turned so extensively (as observed in the evolution of the shear-layer inflection in figure 6) that it is possible that the coflow external to the nozzle had a lesser influence on the shear layer after significant deflection. The spectral character of the elevated jet under these conditions became similar to that of the flush-injected transverse jet at the same low values of R, qualitatively as well as quantitatively (in terms of dominant St values). Just how similar in character the elevated transverse jet's shear-layer behaviour became to that for the flush jet was explored in more detail via low-level jet forcing.

3.3. *Response of shear-layer instabilities to forcing*

Further experiments examined the transverse-jet shear-layer response to low-level sinusoidal jet excitation at various frequencies, for different jet-to-crossflow velocity ratios R and at the two fixed jet Reynolds numbers. Response to low-level excitation has been studied for the free jet (Raman, Rice & Reshotko 1994) and the counterflow jet (Strykowski & Niccum 1991), for example, as a means of exploring the growth or decay of small disturbances. This type of forcing can indicate the possible presence of instabilities which grow spatially and are periodic in time along the shear layer (and hence are convective in nature), in contrast to instabilities that grow in time from the initiation of the layer (and hence may be global or absolutely unstable in nature, as described in Huerre & Monkewitz 1990). Experiments such as the present ones for the transverse jet with $R < 3.5$ or those for the counterflow jet (Strykowski & Niccum 1991), which are unsteady but time invariant in the mean, are characterized by Huerre & Monkewitz (1990) as 'easy' means to explore self-excitation.

Low-level sinusoidal excitation was applied to the jet in the present experiments via the loudspeaker shown in figure 2, at amplitudes that were 10 dB above the unforced jet noise level. This resulted in excitation velocity magnitudes that were less than 1 % of the mean jet velocity. A variety of different applied forcing frequencies f_f were employed in these studies, including those above and below those corresponding to the initial fundamental instability mode frequency f_0 for the given flow conditions.

The spectral characteristics of the upstream jet shear layer for forcing at frequencies f_f that were below f_0, for example, are shown for the flush and elevated transverse jets at $Re = 3000$ in figure 18 for $\infty > R \geqslant 6.4$ and in figure 19 for $4.1 \geqslant R \geqslant 2.0$. Spectra for forced jets at $Re = 2000$ are shown in figure 20 for $\infty > R \geqslant 6.4$, in figure 21 for $4.1 \geqslant R \geqslant 2.0$ and in figure 22 for $1.5 \geqslant R \geqslant 1.15$. The same effects were also observed for values of f_f lying above f_0. The spectral data shown for $Re = 3000$ in figures 18 and 19 may be compared with shear-layer spectra for the non-forced jets in crossflow shown in figures 7 and 8. Similarly, the spectral data shown for $Re = 2000$ in figures 20 to 22 may be compared with shear-layer spectra for the non-forced jets in crossflow shown in figures 9 to 11.

For the free jet ($R \to \infty$), low-level forcing caused excitation of a strong instability at the applied frequency f_f; the fundamental shear-layer frequency f_0 was greatly diminished in strength, barely apparent with the application of such forcing. This type of behaviour is consistent with that of a convectively unstable flow, one in which the dominant instability grows and evolves spatially along the shear layer. This isothermal free jet is well known to exhibit convectively unstable behaviour (Huerre & Monkewitz 1990), and hence the results in figures 18(a, b) and 20(a, b) are consistent with others' observations.

When the crossflow was turned on, the response to low-level forcing at relatively high values of R (e.g. 10 and 6.4) was largely the same as for the free jet, for either flush (figures 18c, e and 20c, e) or elevated (figures 18d, f and 20d, f) injection.

https://doi.org/10.1017/S0022112007008385 Published online by Cambridge University Press

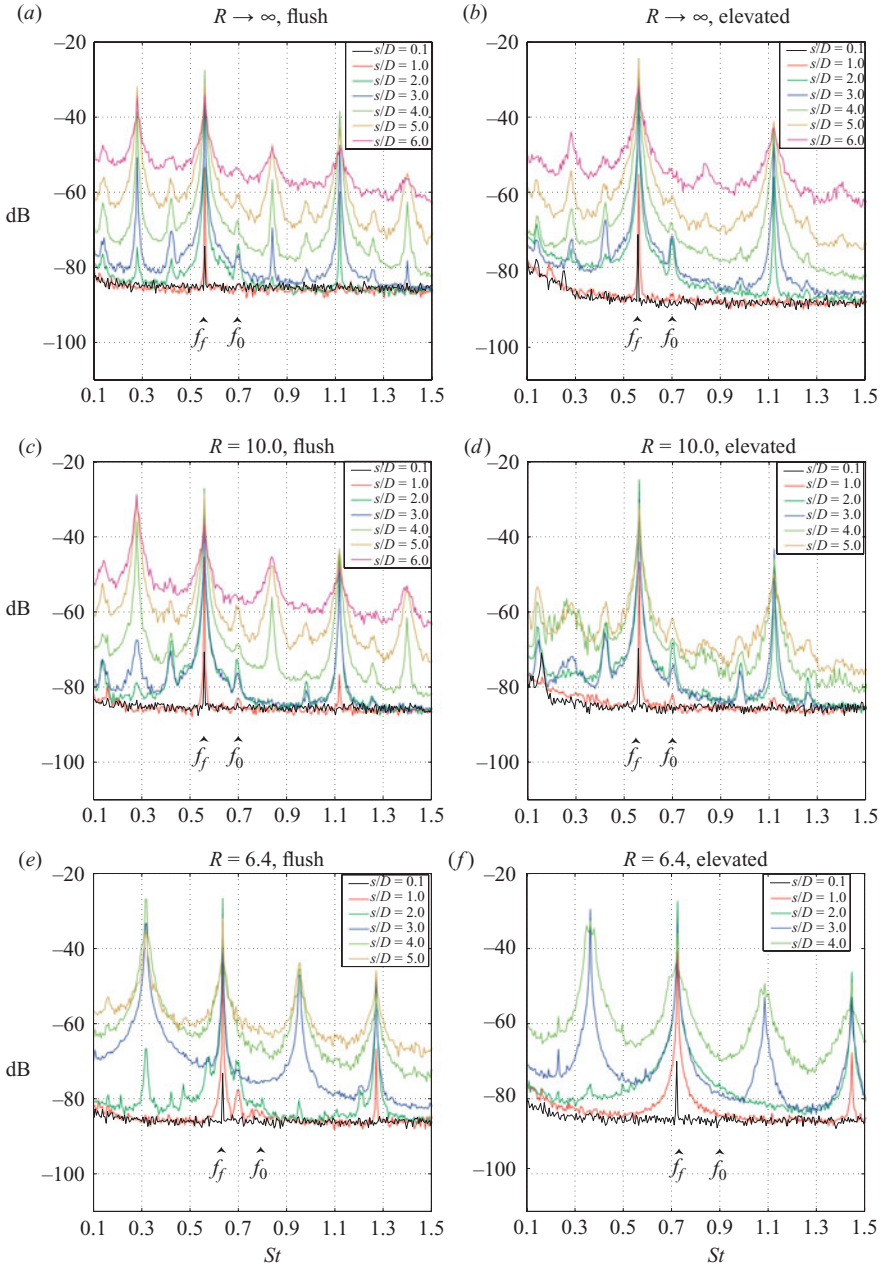


FIGURE 18. Vertical velocity spectra during low-level forcing (at frequencies $f_f < f_0$) for the free (a, b) and transverse jet at various values of the jet-to-crossflow velocity ratio R, measured within the jet shear layer at different distances s from the jet exit. Results for both flush and elevated injection systems are shown. Conditions correspond to a jet Reynolds number of 3000.

Despite the distinctive differences in the spectral character of the unforced transverse jet's shear layer in this regime as compared with that for the free jet, as indicated clearly in the contour plots (figures 13 and 15), the response of the transverse jet shear layer to low-level external forcing at high R remained similar to that for the free

https://doi.org/10.1017/S0022112007008385 Published online by Cambridge University Press

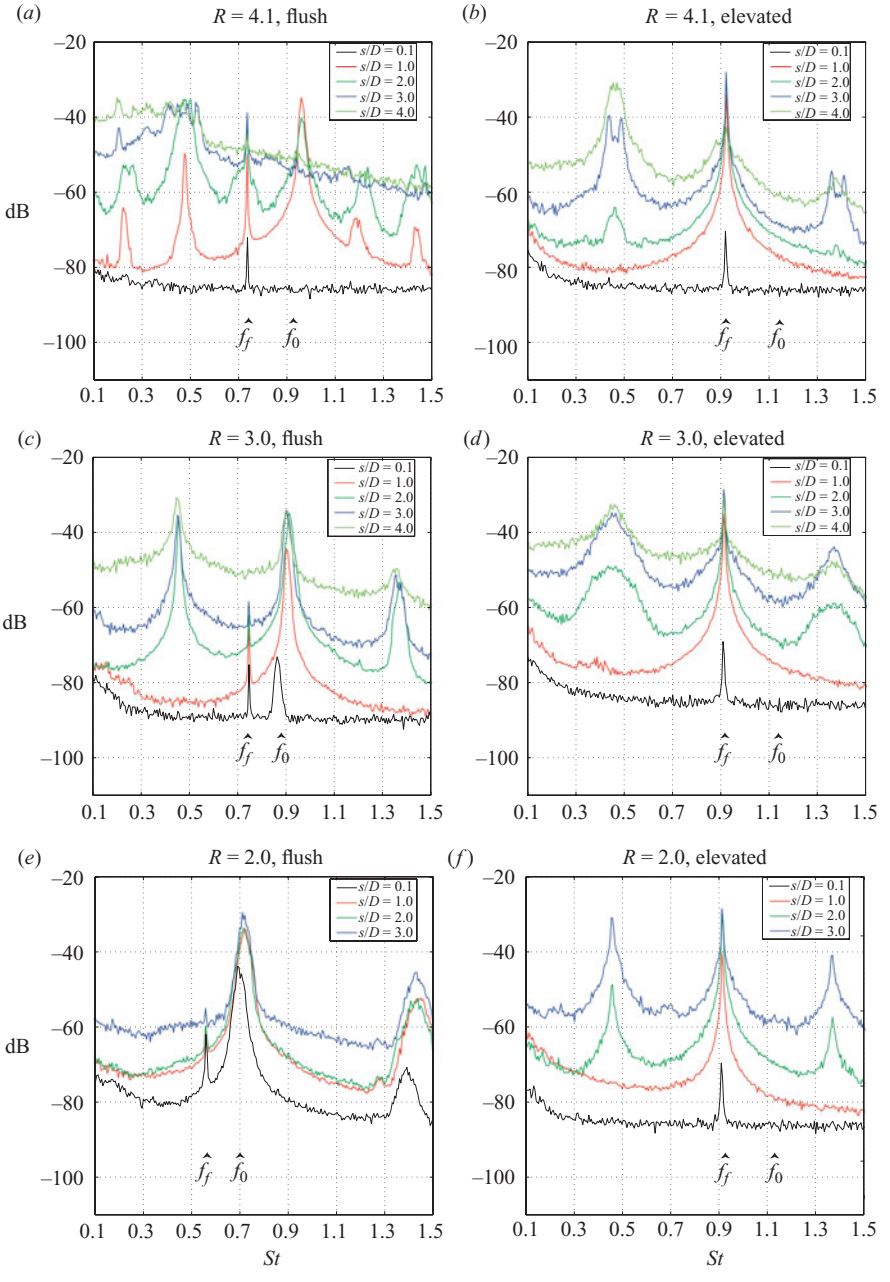


FIGURE 19. Vertical velocity spectra during low-level forcing (at frequencies $f_f < f_0$) for the transverse jet at moderately low values of the jet-to-crossflow velocity ratio R, measured within the jet shear layer at different distances s from the jet exit. Results for both flush and elevated injection systems are shown. Conditions correspond to a jet Reynolds number of 3000.

jet. For all of the forcing conditions examined in this R range, the applied frequency f_f dominated in its influence on the shear layer. For these transverse jets at higher R values, the forcing appeared to enhance the generation of subharmonics as well as higher harmonics to the applied frequency f_f, hence vortex roll-up and pairing

https://doi.org/10.1017/S0022112007008385 Published online by Cambridge University Press

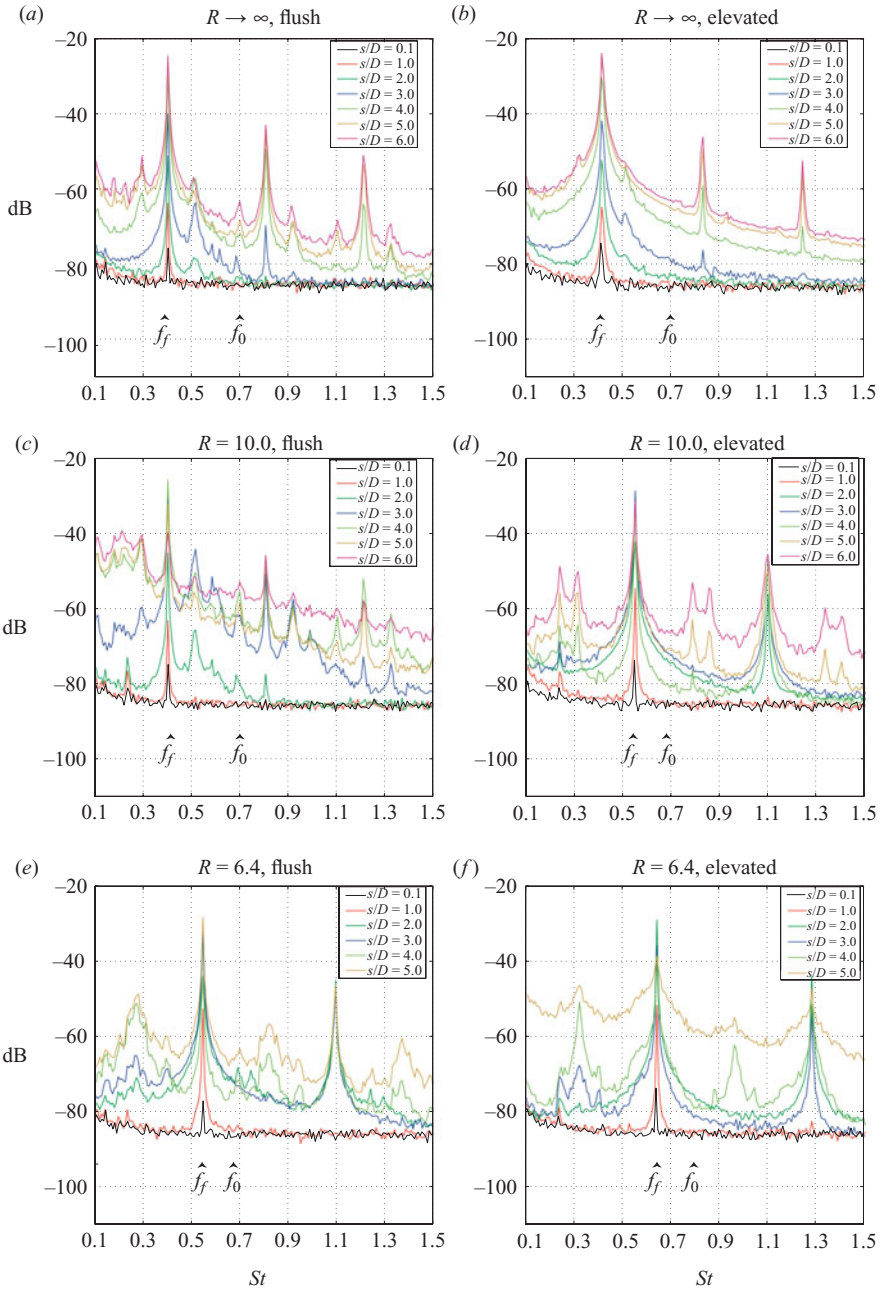


FIGURE 20. As for figure 18, but for a jet Reynolds number of 2000.

phenomena as well as the initiation of nonlinear behaviour were enhanced by such forcing, similar to that observed in forced free shear layers (Ho & Huerre 1984). Although the character of the shear-layer instability was different for the transverse jet with high R as compared with the free jet, the instability itself appeared to remain convective in nature.

https://doi.org/10.1017/S0022112007008385 Published online by Cambridge University Press

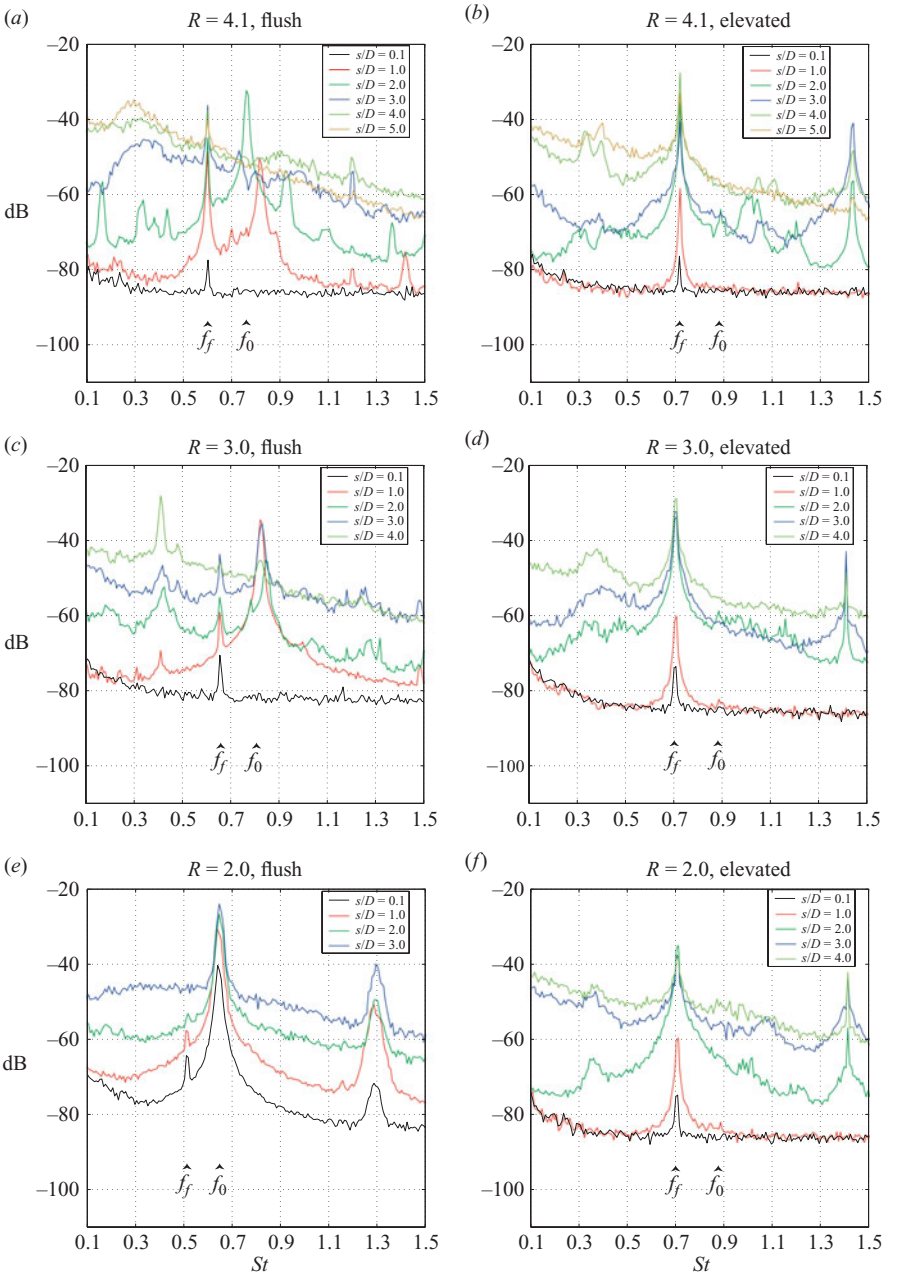


FIGURE 21. As figure 19, but for a jet Reynolds number of 2000.

For the somewhat lower values of R for the flush jet, in the range $4.1 \geqslant R \geqslant 1.15$ as shown in figures 19(a, c, e), 21(a, c, e) and 22(a, c, e), low-level forcing had a weakening influence on the shear layer as compared with its effect at higher R values. In the case of the flush jet, when $R = 4.1$ (figures 19a and 21a), the forcing frequency f_f still became dominant, but the unforced frequency f_0 did not diminish as significantly in strength as it did for transverse jets with a higher R. When R

https://doi.org/10.1017/S0022112007008385 Published online by Cambridge University Press

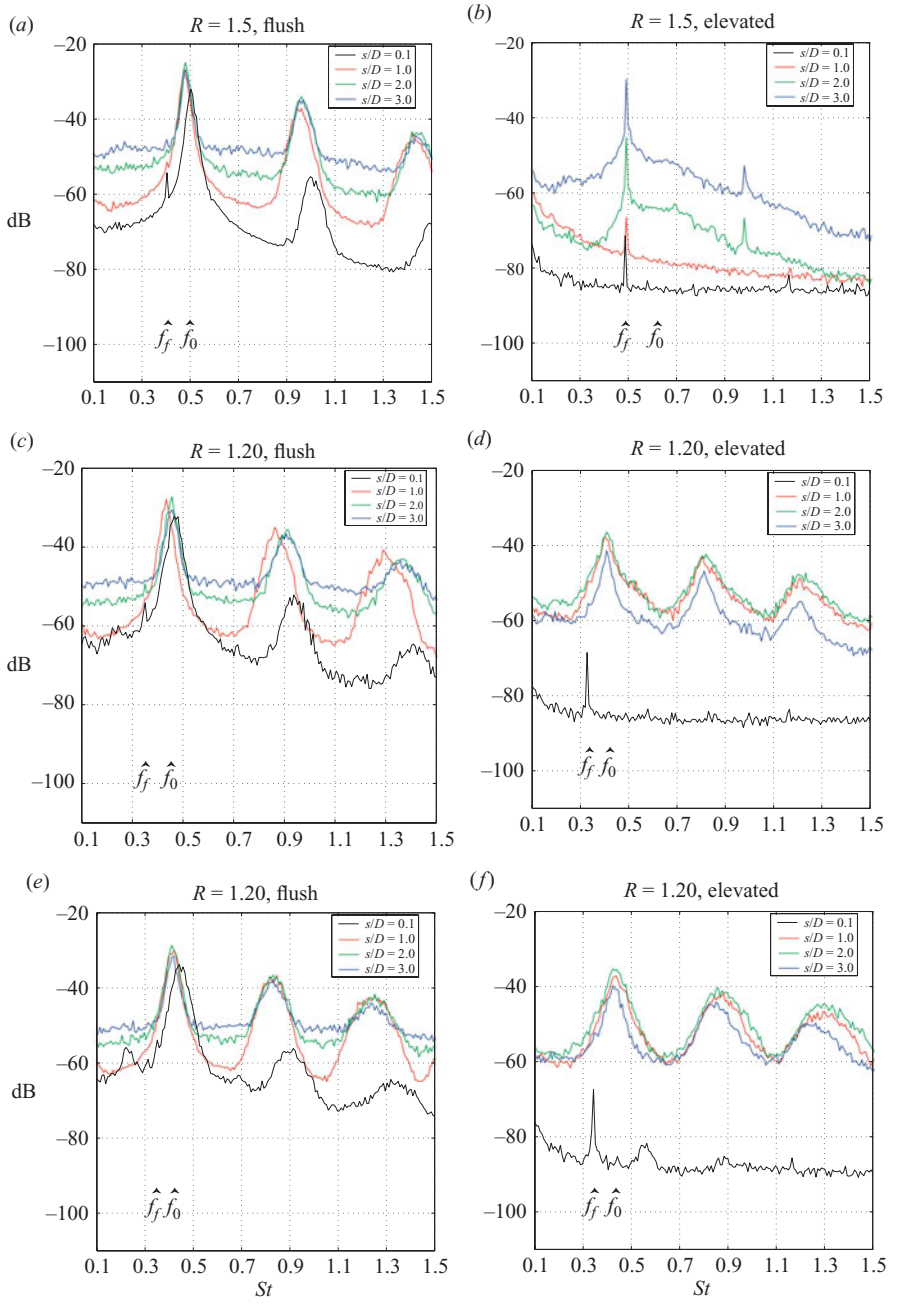


FIGURE 22. Vertical velocity spectra during low-level forcing (at frequencies $f_f < f_0$) for the transverse jet at very low values of the jet-to-crossflow velocity ratio R, measured within the jet shear layer at different distances s from the jet exit. Results for both flush and elevated injection systems are shown. Conditions correspond to a jet Reynolds number of 2000.

was reduced below 3.5 by increasing the crossflow velocity, the unforced transverse jet shear-layer instability was so strong that the applied forcing at f_f had little effect on the shear layer for the flush jet, and the spectra were little altered from the unforced condition. This can be seen by comparing corresponding unforced spectra in

https://doi.org/10.1017/S0022112007008385 Published online by Cambridge University Press

figure 8(c, e) with those in figure 19(c, e), comparing figure 10(c, e) with figure 21(c, e), and by comparing figure 11(a, c, e) with figure 22(a, c, e). In all cases for the flush jet with $R < 3.5$, the strong natural shear-layer modes dominated over the applied forcing frequency. Although not conclusively proved, the shear layer for the flush jet in this regime appeared to exhibit evidence of global self-excitation.

For the elevated transverse jet, in contrast, the applied forcing frequency in the range $4.1 \geqslant R \geqslant 1.25$ still dominated over the unforced mode (see figures 19b, d, f, 21b, d, f and 22b). As with the spectral characteristics for forcing at higher R values, the transverse-jet shear layer exhibited characteristics of a convectively unstable flow, similar to the response of the free jet to such forcing.

In the very low R regime for $Re = 2000$, the elevated jet's response to low-level forcing (shown in figures 22d, f) underwent a transition such that at $R = 1.20$ and below, the applied frequency f_f had a far lesser influence on the shear layer than did the naturally occurring dominant mode with frequency f_0. The behaviour of the elevated transverse jet's shear layer for these very strong crossflow magnitudes became very similar to that of the flush injected transverse jet. For the elevated jet, even with a large degree of coflow for $R < 1.25$, the strong turning of the jet appeared to lessen the impact of the stabilizing influence of the coflow. For the flush-injected jet, a larger crossflow magnitude created a relatively thinner boundary layer upstream of the jet nozzle, allowing greater transverse jet turning, approximately to the same degree as for the elevated jet. The quantitative similarities in the dominant frequencies (and harmonics) between the flush and elevated jets for a given R value in this regime suggest similar flow conditions adjacent to the shear layer for each case, and the remarkable robustness in the spectral character of the transverse jet.

At the beginning of this section, it was noted that low-level shear-layer forcing can be used as a means of exploring the growth or decay of small disturbances. The spatial rate of growth of the shear-layer instability in its initial stage of development (where the disturbances are still linear) may be estimated in the present experiments by looking at the spatial evolution of the measured vertical velocity disturbance amplitude A under non-forced conditions. Assuming the initial disturbance amplitude grows in proportion to $e^{i\alpha s}$ (where $i \equiv \sqrt{-1}$) along the shear layer, the growth rate $-\mathrm{Im}[\alpha]$, with units of inverse length, may be estimated through measurements of the spatial variation in the velocity disturbance amplitude A according to

$$-\mathrm{Im}[\alpha] = \frac{1}{A}\frac{\mathrm{d}A}{\mathrm{d}s} \tag{3.1}$$

A non-dimensional growth rate, $-\mathrm{Im}[\alpha]\theta_u$, may be defined in terms of the upstream shear-layer momentum thickness.

The present experiments were such that the spatial growth rate could be roughly estimated from a least-squares fit of amplitude-variation data along the shear-layer trajectory to an exponential curve for values of R ranging from infinity (the free jet) down to about 4.1 for the flush jet and about 3 for the elevated jet. At smaller jet-to-crossflow velocity ratios, the instabilities evolved so quickly and became so strong in the flush jet, yet were so weakened in the elevated jet, that accurate estimates of growth rate were not possible for either case. Results for the values of the non-dimensional growth rate $-\mathrm{Im}[\alpha]\theta_u$ are shown in figure 23. Again, these should be regarded to be rough estimates, as the value of $-\mathrm{Im}[\alpha]$ could change by as much as 40 % at lower R values ($R < 4$), depending on the number of data points along the trajectory used in the least-squares fit. Just as the Strouhal number for the initial instability appeared to rise with decreasing R for $4 < R \lesssim 8$, so the rate of growth

https://doi.org/10.1017/S0022112007008385 Published online by Cambridge University Press

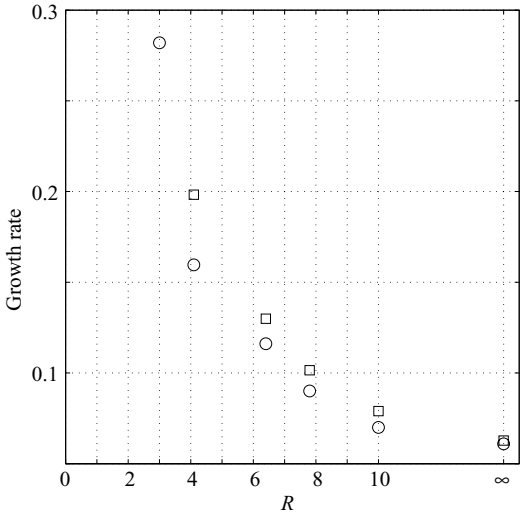


FIGURE 23. Plots of the estimated non-dimensional initial growth rate, $-\mathrm{Im}[\alpha]\theta_u$, for the shear-layer instabilities for different values of the jet-to-crossflow velocity ratio R and for a jet Reynolds number of 2000. Results for both flush (□) and elevated (○) nozzles are shown.

of the instabilities appeared to increase with decreasing R. The differences in growth rates observed between the flush and the elevated nozzles were relatively small. These trends in growth rate with respect to R in this range are also predicted by the local stability analysis described in Part 2. The significant nonlinear rate of growth in the amplitude of the instability for the flush jet with $R \lesssim 4$ provides further evidence of a possible transition to global instability.

4. Discussion and conclusions

The observed transitions in the transverse-jet upstream shear-layer instabilities with a reduction in the jet-to-crossflow velocity ratio R, from infinity (the free jet) down to the order of unity, indicate important differences in the nature of the transverse jet itself. These experiments suggest that even at relatively large values of R, the transverse-jet shear-layer instabilities may be remarkably different from those associated with the free jet. Whether injected from a flush or an elevated nozzle, transverse-jet shear layers for $R > 3.5$ exhibited increasingly strong fundamental instability modes, occurring closer to the jet exit for increasing crossflow magnitudes. The unusual mode-shifting behaviour (e.g. as shown in the contour plots in figure 15) was a robust feature of the shear layer.

Because this distinctive spectral character of the instability was observed for both flush and elevated nozzles under similar operating conditions, with similar quantitative features, it is likely that the observed strengthening and mode shifting of the shear-layer instabilities were independent of the different upstream features of the flush and elevated jets. In other words, shear-layer features such as those characterized in the contour plots, e.g. in figures 15(c–f) and 16(a, b), were probably not the result of the presence of the wall boundary layer, the horseshoe vortices, or the transverse jet's wake vortices (typically associated with flush injection as indicated in figure 1), nor were they likely to be the result of the exterior coflow observed in the elevated jet.

https://doi.org/10.1017/S0022112007008385 Published online by Cambridge University Press

Rather, the unique features of the shear-layer instability were probably fundamental to the transverse jet itself, since they occurred in both injection systems.

In the present experiments, shear-layer instabilities in the range $3.25 \geqslant R \geqslant 1.25$ differed in character between flush- and elevated-injection conditions, and we believe that to a certain extent, some of these differences evolved from the high external coflow experienced by the elevated jets at increasing crossflow velocities. For the present elevated nozzle, the coflow component of velocity exterior to the nozzle became appreciable (greater than 5 % of the mean jet velocity) when R was below about 4, for both Reynolds numbers explored. Below this critical value of R, the elevated jet's shear-layer instabilities were dramatically weakened in comparison to those for the flush jet, at least until R was reduced below 1.25. This regime of weakened instabilities for the elevated transverse jet may actually be dependent on the particular experimental apparatus rather than the R range, in that the magnitude of coflow outside of an elevated nozzle will be different for different nozzle heights with the same crossflow velocity. However, the fact that the elevated jet's shear-layer instabilities became more like those for the flush transverse jet when the elevated jet turned significantly at $R \leqslant 1.20$ speaks to the robustness of the fundamental transverse-jet shear-layer instabilities and their transition during strong crossflow interactions.

The most intriguing aspect of the present study involves the very strong instabilities that form very close to the jet exit for the flush jet in the range where $R < 3.5$. Because similar spectral characteristics were observed for the elevated nozzle for $R \leqslant 1.20$, these strong instabilities were possibly not the result of negative flow (counterflow) in the vicinity of the upstream jet shear-layer owing to wall boundary-layer effects. Such negative flow has been observed for flush-injected transverse jets (e.g. Kelso *et al.* 1996), resulting from the horseshoe vortices and upstream separated flow from the wall boundary layer. Although there was no wall boundary layer in the elevated nozzle experiments, this does not preclude the possibility of negative flow into the nozzle from the strong crossflow, although its source would not be obvious. On the other hand, there is thought to be some negative flow (Kelso *et al.* 1996) associated with the transverse jet's 'hovering vortex' structure, and this could be relevant to the observed transitions in the instabilities for both injection systems. The hovering vortex is thought to become stronger as the crossflow velocity is increased (for lower R values), but the structure is still understood to hover about the transverse jet, remaining decoupled from the wall-associated horseshoe vortices.

Differences in the response to low-level forcing by the transverse-jet shear layer as the jet-to-crossflow velocity ratio R is reduced, offer intriguing possibilities for understanding the differences summarized above. The shear-layer response to forcing may relate to a transition in the nature of the convectively unstable flow at higher values of R to a globally or absolutely unstable flow at lower values of R. This transition may be similar, for example, to that observed by Monkewitz *et al.* (1990) for the heated laminar or transitional axisymmetric free jet as compared with the isothermal free jet. Yet as noted by Huerre & Monkewitz (1990), the present experimental approach in examining shear-layer instabilities (exploring spectral differences and response to low-level forcing) constitute a class of experiments that yield only supporting evidence for the transition to self-excitation. Our results do not offer conclusive evidence of this type of transition for the transverse jet, only the possibility that it might be taking place.

These differences in the transverse-jet shear-layer response for different jet and crossflow conditions suggest that a variety of different jet forcing strategies could be applied for the control of such jets in practical systems, depending on the specific

https://doi.org/10.1017/S0022112007008385 Published online by Cambridge University Press

jet and crossflow conditions present and the specific flow regime. For example, for transverse jets with a larger R value (above 3.5), relatively low-level excitation could be employed to promote mixing by excitation of the convective instability without actually increasing the crossflow velocity. This is a possible explanation for the observations of Narayanan *et al.* (2003) which suggest that sinusoidal excitation could enhance transverse jet mixing for $R = 6$. On the other hand, at lower values of R, below 4, where the unforced jet exhibits stronger dominant modes, low-level excitation would have a relatively small impact on the jet and its evolution. The jet under these conditions may already be self-excited. This finding may also explain our group's earlier observations (M'Closkey *et al.* 2002; Shapiro *et al.* 2006) for $R \leqslant 4$, that even large-scale sinusoidal excitation has little effect on jet penetration, spread and, probably, mixing. For these low R values, imposition of stronger forcing, especially with a distinct, externally imposed time scale such as that created by square-wave excitation with a prescribed temporal pulsewidth, may be required to impact jet penetration and spread. In this regime, the impact of strong-vorticity generation (and ultimate breakdown) may be more critical to mixing. These differences in the stability characteristics of the jet in crossflow suggest the benefits of a 'two-pronged' approach to the control of transverse-jet penetration, mixing and spread, which will be the focus of future studies.

The authors wish to acknowledge the contributions of Professors Robert Kelly and Robert M'Closkey of UCLA, Professor Luca Cortelezzi of McGill University, and of UCLA students Marcus George, Edson Rodriguez, Kristy Dalrymple, Rebekah Tanimoto, Stephan Shahinian, Lydia Trevino and Priya Sheth in various stages of these studies. Support for this project from the National Science Foundation under grants CTS-0200999 and CTS-0457413, and from NASA Dryden Flight Research Center under grant NCC-157, is gratefully acknowledged.

REFERENCES

Alves, L., Kelly, R. E. & Karagozian, A. R. 2007*a* Local stability analysis of an inviscid transverse jet. *J. Fluid Mech.* **581**, 401–418.

Alves, L., Kelly, R. E. & Karagozian, A. R. 2007*b* Transverse jet shear layer instabilities. Part 2. Linear analysis for large jet-to-crossflow velocity ratio. *J. Fluid Mech.* (submitted).

Andreopoulos, J. 1985 On the structure of jets in a crossflow. *J. Fluid Mech.* **157**, 163–197.

Blanchard, J. N., Brunet, Y. & Merlen, A. 1999 Influence of a counter rotating vortex pair on the stability of a jet in crossflow: an experimental study by flow visualizations. *Exps. Fluids* **26**, 63–74.

Broadwell, J. E. & Breidenthal, R. E. 1984 Structure and mixing of a transverse jet in incompressible flow. *J. Fluid Mech.* **148**, 405–412.

Camussi, R., Guj, G. & Stella, A. 2002 Experimental study of a jet in a crossflow at very low Reynolds number. *J. Fluid Mech.* **454**, 113–144.

Cortelezzi, L. & Karagozian, A. R. 2001 On the formation of the counter-rotating vortex pair in transverse jets. *J. Fluid Mech.* **446**, 347–373.

Eroglu, A. & Breidenthal, R. E. 2001 Structure, penetration, and mixing of pulsed jets in crossflow. *AIAA J.* **39** (3), 417–423.

Fric, T. F. & Roshko, A. 1994 Vortical structure in the wake of a transverse jet. *J. Fluid Mech.* **279**, 1–47.

Gharib, M., Rambod, E. & Shariff, K. 1998 A universal time scale for vortex ring formation. *J. Fluid Mech.* **360**, 121–141.

Ho, C. M. & Huerre, P. 1984 Perturbed free shear layers. *Annu. Rev. Fluid Mech.* **16**, 365–424.

Holdeman, J. D. 1993 Mixing of multiple jets in a confined subsonic crossflow. *Prog. Energy Combust. Sci.* **19**, 31–70.

https://doi.org/10.1017/S0022112007008385 Published online by Cambridge University Press

Huerre, P. & Monkewitz, P. A. 1990 Local and global instabilities in spatially developing flows. *Annu. Rev. Fluid Mech.* **22**, 473–537.

Johari, H., Pacheco-Tougas, M. & Hermanson, J. C. 1999 Penetration and mixing of fully modulated turbulent jets in crossflow. *AIAA J.* **37**, 842–850.

Kamotani, Y. & Greber, I. 1972 Experiments on a turbulent jet in a cross flow. *AIAA J.* **10**, 1425–1429.

Karagozian, A. R. 1986 An analytical model for the vorticity associated with a transverse jet. *AIAA J.* **24**, 429–436.

Kelso, R. & Smits, A. 1995 Horseshoe vortex systems resulting from the interaction between a laminar boundary layer and a transverse jet. *Phys. Fluids* **7**, 153–158.

Kelso, R. M., Lim, T. T. & Perry, A. E. 1996 An experimental study of round jets in cross-flow. *J. Fluid Mech.* **306**, 111–144.

Kibens, V. 1981 The limit of initial shear layer influence on jet development. *AIAA Paper* 81-1960.

King, J. M. 2002 The actively controlled jet in crossflow. Master's thesis, University of California, Los Angeles, Department of Mechanical and Aerospace Engineering.

M'Closkey, R. T., King, J., Cortelezzi, L. & Karagozian, A. R. 2002 The actively controlled jet in crossflow. *J. Fluid Mech.* **452**, 325–335.

Margason, R. J. 1993 Fifty years of jet in cross flow research. *AGARD CP* 534 **1**, 1–141.

Megerian, S. & Karagozian, A. R. 2005 Evolution of shear layer instabilities in the transverse jet. In *43rd AIAA Aerospace Sci. Conf.* Paper 2005-0142.

Michalke, A. 1971 Instabilität eines kompressiblen runden freistrahls unter berücksichtigung des einflusses der strahlgrenzschichtdicke. *Z. Flugwiss.* **19** (8–9), 319–328. In English: *NASA TM* 75190 (1977).

Michalke, A. & Hermann, G. 1982 On the inviscid instability of a circular jet with external flow. *J. Fluid Mech.* **114**, 343–359.

Monkewitz, P. A., Bechert, D. W., Barsikow, B. & Lehmann, B. 1990 Self-excited oscillations and mixing in a heated round jet. *J. Fluid Mech.* **213**, 611–639.

Moussa, Z. M., Trischka, J. W. & Eskinazi, S. 1977 The nearfield in the mixing of a round jet with a cross-stream. *J. Fluid Mech.* **80**, 49–80.

Narayanan, S., Barooah, P. & Cohen, J. M. 2003 Dynamics and control of an isolated jet in crossflow. *AIAA J.* **41**, 2316–2330.

Petersen, R. A. & Samet, M. M. 1988 On the preferred mode of jet instability. *J. Fluid Mech.* **194**, 153–173.

Peterson, S. D. & Plesniak, M. W. 2004 Evolution of jets emanating from short holes into crossflow. *J. Fluid Mech.* **503**, 57–91.

Raman, G., Rice, E. J. & Reshotko, E. 1994 Mode spectra of natural disturbances in a circular jet and the effect of acoustic forcing. *Exps Fluids* **17**, 415–426.

Rudman, M. 1996 Simulation of the near field of a jet in cross flow. *Expl Thermal Fluid Sci.* **12**, 134–141.

Schuller, T., King, J., Majamaki, A. & Karagozian, A. R. 1999 An experimental study of acoustically controlled gas jets in crossflow. *Bull. Am. Phys. Soc.* **44**, 111.

Shapiro, S. R. 2003 Optimization of controlled jets in crossflow. Master's thesis, University of California, Los Angeles, Department of Mechanical and Aerospace Engineering.

Shapiro, S., King, J., M'Closkey, R. T. & Karagozian, A. R. 2006 Optimization of controlled jets in crossflow. *AIAA J.* **44**, 1292–1298.

Smith, S. H. & Mungal, M. G. 1998 Mixing, structure and scaling of the jet in crossflow. *J. Fluid Mech.* **357**, 83–122.

Strykowski, P. J. & Niccum, D. L. 1991 The stability of countercurrent mixing layers in circular jets. *J. Fluid Mech.* **227**, 309–343.

Vermeulen, P. J., Grabinski, P. & Ramesh, V. 1992 Mixing of an acoustically excited air jet J: with a confined hot crossflow. *Trans. ASME* J: *Engng. Gas Turbines Power* **114**, 46–54.

Xu, G. & Antonia, R. A. 2002 Effect of different initial conditions on a turbulent round free jet. *Exps Fluids* **33**, 677–683.

Yuan, L. L. & Street, R. L. 1998 Trajectory and entrainment of a round jet in crossflow. *Phys. Fluids* **10**, 2323–2335.

https://doi.org/10.1017/S0022112007008385 Published online by Cambridge University Press